Above- and Belowground Plant Mercury Dynamics in a Salt Marsh Estuary in Massachusetts, USA

Ting Wang[1], Buyun Du[1,2], Inke Forbrich[3,4], Jun Zhou[1,5], Joshua Polen[1], Elsie M. Sunderland[6], Prentiss H. Balcom[6], Celia Chen[7], Daniel Obrist[1,8*]

[1]Department of Environmental, Earth, and Atmospheric Sciences, University of Massachusetts Lowell, Lowell, MA 01854, USA

[2]College of Environment and Ecology, Jiangsu Open University, Nanjing, 210005, China

[3]Marine Biological Laboratory, Woods Hole, MA 02543, USA

[4]Department of Environmental Sciences, The University of Toledo, Toledo, OH 43606, USA

[5]Key Laboratory of Soil Environment and Pollution Remediation, Institute of Soil Science, Chinese Academy of Sciences, Nanjing 210008, China

[6]Harvard John A. Paulson School of Engineering and Applied Sciences, Harvard University, Cambridge, MA 02138, USA

[7]Department of Biological Sciences, Dartmouth College, Hanover, NH 03755, USA

[8]Division of Agriculture and Natural Resources, University of California, Davis, CA 95618, USA

Correspondence to: Daniel Obrist (daniel_obrist@uml.edu)

Abstract. Estuaries are a conduit of mercury (Hg) to from watersheds to the coastal ocean, and salt marshes play an important role in coastal Hg cycling. Hg cycling in upland terrestrial ecosystems have been well studied, but processes in densely vegetated salt marsh ecosystems are poorly characterized. We investigated Hg dynamics in vegetation and soils in the Plum Island Sound estuary in Massachusetts, USA, and specifically assessed the role of marsh vegetation for Hg deposition and turnover. Monthly quantitative harvesting of aboveground biomass showed strong linear seasonal increases in Hg associated with plants, with a four-fold increase in Hg concentration and an eight-fold increase in standing Hg mass from June (3.9 ± 0.2 µg kg^{-1} and 0.7 ± 0.4 µg m^{-2}, respectively) to November (16.2 ± 2.0 µg kg^{-1} and 5.7 ± 2.1 µg m^{-2}, respectively). Hg did not increase further in aboveground biomass after plant senescence, indicating physiological controls of vegetation Hg uptake in salt marsh plants. Hg concentrations in live roots and live rhizomes were 11 times and two times higher than concentrations in aboveground live biomass, respectively. Furthermore, live belowground biomass Hg pools (Hg in roots and rhizomes, 108.1 ± 83.4 µg m^{-2}) were more than ten times larger than peak standing aboveground Hg pools (9.0 ± 3.3 µg m^{-2}).

A ternary mixing model of measured stable Hg isotopes suggests that Hg sources in marsh aboveground tissues originate from about equal contributions of root uptake (~35%), precipitation uptake (~33%), and atmospheric gaseous elemental mercury (GEM) uptake (~32%). These results suggest a more important role of Hg transport from belowground (i.e., roots) to aboveground tissues in salt marsh vegetation than upland vegetation, where GEM uptake is generally the dominant Hg source. Roots and soils showed similar isotopic signatures suggesting that belowground tissue Hg mostly derived from soil uptake. Annual root turnover results in large internal Hg recycling between soils and plants, estimated at 58.6 µg m^{-2} yr^{-1}. An initial mass balance of Hg indicates that the salt marsh presently serves as a small net Hg sink for environmental Hg of 5.2 µg m^{-2} yr^{-1}.

1. Introduction

Coastal salt marshes are located at the interface between terrestrial and marine ecosystems and undergo diurnal saltwater inundation by tidal water. They provide important ecological services, have high socioeconomic benefits, and serve as sinks and sources of carbon, nutrients, and contaminants (Hopkinson et al., 2018; Morris et al., 2013). They are at the interface of rivers and oceans,

whereby rivers annually transport approximately 27 ± 13 Mmol yr^{-1} of mercury (Hg) to coastal oceans globally (mostly deposited to estuarine regions (Amos et al., 2014; Liu et al., 2021; Zhang et al., 2015). The location of salt marshes at this interface merits an understanding of their respective Hg sinks and sources and role in coastal Hg cycling. The site of this study was within the Plum Island Sound salt marsh in Massachusetts, USA, the largest macrotidal marsh estuary in New England. The area has been considered a biological mercury (Hg) hotspot, with 62% of saltmarsh sparrows reportedly exceeding a blood Hg threshold that may reduce nesting success (Evers et al., 2007; Jackson et al., 2011; Lane et al., 2020; Lane et al., 2011), although reasons for high Hg exposure are not fully understood. A potentially important Hg source in marshes includes Hg uptake by plants. In terrestrial environments, plants assimilate substantial amounts of atmospheric Hg, which is subsequently transferred to soils via tissue senescence (e.g., litterfall) and wash-off (i.e., throughfall deposition) (Fisher and Wolfe, 2012; Iverfeldt, 1991; Rea et al., 1996; Zhou et al., 2021). This plant Hg uptake is considered dominated by assimilation of atmospheric gaseous elemental Hg (GEM), so that global vegetation acts as a large atmospheric GEM pump to soils (Fu et al., 2019; Jiskra et al., 2018; Obrist et al., 2018; Wang et al., 2019, 2022; Zhou et al., 2021; Zhou and Obrist, 2021). In terrestrial ecosystems, Hg inputs derived from plants are the dominant Hg sources accounting for 60% to 90% of the total Hg inputs to soils (Zhou and Obrist, 2021). Salt marshes are characterized by high plant net primary productivity (NPP) driven by vascular macrophytes, with plant NPP as high and even exceeding that of terrestrial ecosystems (Marques et al., 2011;Tobias and Neubauer, 2009; Visser et al., 2018). For example, salt marsh biomass production across Atlantic and Gulf sites in the U.S. ranges from 228 to 1,335 g C m^{-2} yr^{-1} with a median value of 537 g C m^{-2} yr^{-1} (Tobias and Neubauer, 2009). By comparison, NPP across 18 productive U.S. forests ranging between 400 to 1,000 g C m^{-2} y^{-1} (He et al., 2012). As salt marshes are considered strong sinks of atmospheric carbon driven by plant CO$_2$ assimilation (Forbrich et al., 2018), their high NPP also may lead to increased deposition of atmospheric Hg due to vegetation assimilation of atmospheric Hg and subsequent transfer to salt marsh ecosystems via litterfall and plant senescence.

We hypothesized that salt marsh plants in the Plum Island estuary salt marsh act as substantial sinks of atmospheric Hg via vegetative assimilation of GEM, and aimed to quantify Hg sources in salt marsh vegetation, accumulation rates, and turnover rates of Hg in salt marsh plants. We quantified Hg fluxes and pools associated with plant dynamics in the salt marsh and Hg associated with annual growth of aboveground tissues, estimated transfer of Hg associated with aboveground tissues to soils, and assessed Hg turnover in belowground biomass. In addition, we quantified specific sources of Hg in salt marsh biomass tissues using stable Hg isotope signatures, with isotope endmembers representing different sources such as plant uptake of atmospheric elemental, root uptake of soil Hg, and precipitation-derived deposition whereby precipitation Hg may include direct deposition to leaves or uptake from soil water (Jiskra et al., 2018; Niu et al., 2011; Zheng et al., 2016).

2. Methods

2.1. Site Description

Sampling sites were located in the Plum Island Sound on the northeastern coast of Massachusetts, USA (42°45'10", 70°56'46") between the Gulf of Maine and the city of Boston. The estuary is the largest marsh-dominated estuary in New England with a total marsh area of 60 km^2 and salt marsh area of 40 km^2 (Hopkinson et al., 2018; Millette et al., 2010). Tides are semidiurnal with an amplitude averaging 2.7 m (NOAA Tide Predictions, 2020). We focused our study on high marsh platforms, with an approximate elevation of 1.4 m above the North American Vertical Datum 88, which dominate tidal marshes in New England and accounts for 75% of the vegetated area in the Plum Island Sound estuary (Millette et al., 2010; Wilson et al., 2014). The high marsh exhibits poor water drainage (Wilson et al., 2014) and is generally inundated biweekly during spring tides and during major storms (Millette et al., 2010). The two dominant species on the high marsh are C4 species including *Sporobolus pumilus* (common name: marsh

hay) and *Sporobolus alterniflorus* (common name: smooth cordgrass), with the latter mainly distributed along tidal channels and also dominant in low marsh platforms (Anjum et al., 2012; Cheng et al., 2006; Curtis et al., 1990; Maricle et al., 2009; Sun et al., 2020). Another C4 species, *Distichlis spicata* (coastal saltgrass), is often collocated within *S. pumilus* -dominated sites on high marsh platforms (Arp et al., 1993), whereas *Juncus gerardii* (saltmarsh rush) usually dominates the terrestrial boundary of the high marsh (Bertness, 1991).

Although the upland watershed of this salt marsh does not have any known point sources of Hg, previous studies pointed to the possibility of legacy anthropogenic sources present in this marsh estuary, possibly from ocean water import of Hg from nearby riverine sources, and other possible sources include regional atmospheric deposition directly to the marsh and its watershed (Evers et al., 2007; Lane et al., 2020; Lane et al., 2011; Wang and Obrist, 2022). A previous of our group showed high Hg concentrations observed in marsh soils and evidence that the salt marsh soils currently serve as a source of Hg to tidal water and the nearby ocean dominated lateral particulate-bound Hg transport (Wang and Obrist, 2022). However, a comprehensive mass balance of Hg inputs and outputs in this system is currently missing.

2.2. Sampling and Processing of Vegetation and Soil

Aboveground biomass of the dominant species, *S. alterniflorus* and *S. pumilus*, were collected every four to five weeks between June and November in 2021, corresponding to the active growing season. Additional senesced biomass was sampled in the following year in April 2022, and two additional salt marsh species, *D. spicata* and *J. gerardii,* were sampled in September 2018. For each sampling date, eight 1-m^2 square plots were selected in the footprint area of a micrometeorological flux tower (Forbrich et al., 2018), of which four squares were dominated by *S. alterniflorus* and four adjacent squares were dominated by *S. pumilus*. During vegetation sampling, all aboveground vegetation within the 1-m^2 squares was clipped close to the ground and stored in plastic Ziploc bags in coolers over ice and subsequently in refrigerators until processing. In the laboratory, wet and dry vegetation mass was determined, and vegetation was carefully separated into live and senesced tissues. Note that in these ecosystems, significant amounts of senesced standing tissues from the previous year are present along with current year green tissues. We then prepared the samples for analysis of Hg in both bulk samples and in individual species.

In four of the eight sampling sites, quantitative belowground sampling was performed in July 2021, with two plots dominated by *S. alterniflorus* and the other two plots dominated by *S. pumilus*. Soil cores with diameter of 10 cm to a depth of 40 cm were taken and separated into depth increments of 0-20 cm and 20-40 cm. Belowground components were separated into the following components by washing onto a fine mesh with pore size of 0.25 mm: live roots and rhizomes identified by turgidity and color (e.g., hard and white tissues versus soft and grey/discolored); senesced roots, rhizomes, and soil detritus (not recognizable organic matter); and sediments and fine organic matter that passed through the fine mesh (only analyzed in two subsamples). This process was based on visual separation of tissues (Elsey-Quirk et al., 2011; Valiela et al., 1976). We observed live roots and rhizomes only in the top 20 cm of the soils with no recognizable live roots and rhizomes at 20-40 cm depth. All plant tissues were rinsed with tap water until the water was clean, then thoroughly rinsed three times with Milli-Q water, while a selected number of live aboveground tissues were analyzed both washed and unwashed for estimation of washable Hg (see section of throughfall estimation). All samples were dried at 65 °C to reach a constant weight and were milled and homogenized using stainless steel coffee grinders (for vegetation samples) and 8530 Shatter-Box (for soil samples) prior to analyses. The coffee grinders and Shatter-Box were rinsed with Milli-Q water and dried with Kimwipes between samples.

2.3. Hg concentration and stable isotope analysis of vegetation and soils samples

Total Hg concentrations in all components were measured using a tri-cell Milestone DMA-80 Direct Mercury Analyzer (Milestone Inc., Monroe, Connecticut, USA) through thermal decomposition, catalytic reduction, amalgamation, desorption, and atomic absorption spectroscopy following EPA method 7473 (U.S. EPA., 1998). The system was re-calibrated based on daily performance checks using five-point calibration curves. Standard reference materials, including NIST 1515 Apple leaves (43.2 µg kg^{-1}) and Canadian National Research Council certified reference material MESS-4 (marine sediment, 91 µg kg^{-1}), were used as continuous calibration verifications after every ten-samples. Percent recoveries of total Hg for certified reference materials averaged of 99.9 ± 5.5% (range of 89.6% to 111.4%) and all blanks were below detection limits (0.001 ng). All samples were analyzed in triplicate and results were accepted when coefficients of variation were less than 10%.

Hg stable isotopes were measured on select samples including live aboveground biomass, live root, live rhizomes, and surface (0-22.5 cm) and deeper soils (97.5 cm). Samples were pre-concentrated with a Nippon direct Hg analyzer (Nippon Instruments) as described in Enrico et al. (2021). A HGX-200 cold vapor generator (Teledyne Cetac Technologies) was used to introduce sample Hg to a Thermo Neptune plus MC-ICP-MS at Harvard University. An Apex-Q nebulizer (Elemental Scientific) was used to nebulize a Thallium (Tl) solution and inject TI aerosols in the HGX-200. NIST3133 (primary standard) and RM8610 (previously UM- Almaden, secondary standard) were used as Hg isotopic standard solutions, and NIST997 (thallium isotopic standard solution) was used as the reference material to correct instrument mass bias. NIST 1515 Apple leaves and Canadian National Research Council certified reference material MESS-4 were used to verify isotope analysis, and standard recoveries were in the acceptable range (from 82% to 93%). For analysis on Neptune, all trapped samples and standards were diluted with trapping solution to either 1 or 2 ng mL^{-1}, which concentrations could be matched with NIST 3133 bracketing standard and the UM-Almaden concentrations. Quality control results for MESS-4 and RM8610 were similar to previously published findings (Table S4, Blum and Johnson, 2017; Enrico et al., 2021). Small delta (δ) annotation is used for mass-dependent fractionation (MDF), which is reported as per mil (‰) values relative to NIST-3133 based on equation (1),

$$\delta^{xxx}Hg = \left(\frac{(^{xxx}Hg/^{198}Hg)_{sample}}{(^{xxx}Hg/^{198}Hg)_{NIST3133}} - 1 \right) \times 1000 \tag{1}$$

where ^{xxx}Hg is the mass of each Hg isotope between 199 and 204. Capital delta (Δ) annotation is used for mass-independent fractionation (MIF), describing fractionation away from the expected MDF based on equation (2),

$$\Delta^{xxx}Hg = \delta^{xxx}Hg - \beta_{xxx} \times \delta^{202}Hg \tag{2}$$

where ^{xxx}Hg denotes mass of each Hg isotope 199, 200, 201, and 204, and β_{xxx} is the constant mass-dependent correction factor (0.252, 0.502, 0.752, and 1.492, respectively; Blum and Bergquist, 2007). To determine Hg sources, a ternary isotope mixing model was used to estimate fractions of Hg in above-ground biomass. End-member Hg sources used included signatures of salt marsh plants roots measured in this study, published signatures of upland foliage samples as a proxy for atmospheric GEM uptake and its fractionation during plant uptake, and published date of precipitation Hg (see SI for details). We estimated uncertainty in the mixing model using the variance in precision estimates using Monte Carlo simulations (10,000 trials), with details of the simulation provided in SI (Table S5).

2.4 Data Analysis

Data were checked for normality (Shapiro–Wilk test) and homogeneity of variance assumptions of statistical tests. The non-normalized data were subjected to a natural logarithmic transformation to ensure a normal distribution. Unpaired Student t-tests were used to assess significant differences between groups (e.g., species), and statistical differences between non-washed and

washed aboveground vegetation samples were performed using paired Student t-tests. Linear regression analyses were performed to determine the rate of aboveground biomass Hg uptake over time. Hg mass and turnover rates were calculated by multiplication of Hg concentrations by corresponding biomass or biomass growth and other mass components at the level of sampling plots. All statistical tests were performed with STATA (Version 16.0, Statacorps, College Station, Texas), the mixing model and its uncertainty calculation was performed using Python (Python 3.12.0), and all regressions and statistical tests presented in text, tables, and figures were based on statistical differences with p-values < 0.05. The variability presented in the text and figures is one standard deviation of the means.

3. Results

3.1 Hg concentrations in aboveground and belowground biomass

Hg concentrations in aboveground tissues showed substantial seasonal variations and species-specific differences, with lowest concentrations in live tissues of *S. alterniflorus* and *D. spicata*, followed by *S. pumilus,* and highest concentrations in *J. gerardii* (Fig 1a). Despite species differences in Hg concentrations, concentrations in bulk vegetation of communities dominated by *S. alterniflorus* versus *S. pumilus* (Fig 1b) were not statistically different. This likely occurred because both communities are composed of multiple species. For example, *S. alterniflorus* communities also have a presence of *S. pumilus* plants*, while *S. pumilus* communities include large numbers of *D. spicata* plants. Similarly, Hg concentrations of senesced *S. pumilus* and *S. alterniflorus* bulk samples were not statistically significantly different from each other (Fig S1).

Hg concentrations in aboveground live biomass strongly increased throughout the growing season between June and November across all species. Figure 2 shows linear increases of Hg concentrations in live aboveground tissues in plots dominated by *S. alterniflorus* and *S. pumilus* over time (r^2 = 0.84; p < 0.01; n = 50), with no significant difference in regressions between the two communities. Based on these linear regression slopes, we estimated daily uptake rates of Hg during the growing season of 0.08±0.01 µg kg^{-1} day^{-1} for both *Sporobolus* communities. After senescence, Hg concentrations in senesced aboveground biomass measured in spring of the following year (April 2022) were not further enhanced compared to live biomass samples collected in fall (November 2021; *p* = 0.19), (Figs 2 and 4a) suggesting that no statistically significant Hg uptake (or loss) occurred in biomass after senescence.

Hg concentrations in live roots and rhizomes (upper 20 cm) were two to three times higher in *S. pumilus* plots (258.9±70.3 µg kg^{-1} and 46.6±14.2 µg kg^{-1} respectively) compared to *S. alterniflorus* plots (84.5±47.0 µg kg^{-1} and 27.9±1.1 µg kg^{-1} respectively) (Fig 3, Table S1). In belowground tissues, Hg concentrations were higher in senesced biomass, including dead roots, dead rhizomes, and detritus, compared to live tissues. Belowground tissues also showed higher Hg concentrations than separated soil mineral and humus fractions (although only measured in one *S. pumilus* sample) (Fig 3, Table S1). Bulk soil Hg concentrations (i.e., composed of all fractions listed above) averaged 194.6±28.3 µg kg^{-1} of *S. alterniflorus* community and 171.2±72.1 µg kg^{-1} of *S. pumilus* community in the top 20 cm with no significant difference (p>0.05). Bulk soil Hg concentrations of the 20-40 cm soil in *S. alterniflorus* (279.1±203.8 µg kg^{-1}) were almost twice that of *S. pumilus* (159.1±122.7 µg kg^{-1}). Overall, Hg concentrations of live roots (171.7±111.9 µg kg^{-1}) were 11 times higher and live rhizome (37.3±13.6 µg kg^{-1}) were double the concentrations of aboveground live biomass (16.2±2.0 µg kg^{-1}, Table S2).

3.2 Hg pools sizes associated with aboveground and belowground biomass

Aboveground standing live biomass strongly increased from June through August, when it plateaued at a peak biomass in August (507±208 g m^{-2}) and September (498±118 g m^{-2}, a trend that was consistent among the investigated communities) (Fig 4b). Hg

mass contained in live aboveground biomass peaked later (in November) than standing biomass and showed an eight-fold and near-linear increase between June (0.7 ± 0.4 µg m^{-2}) and November (5.7 ± 2.1 µg m^{-2}) (Fig 4c). Peak Hg pools contained in aboveground biomass were 5.7 ± 2.1 µg m^{-2} for live tissue and 3.3 ± 1.7 µg m^{-2} for senesced tissue, for a total combined standing aboveground biomass Hg pools of 9.0 ± 3.3 µg m^{-2} in November (Figs 4c and 5). This number represents our best estimate of total annual Hg assimilation by aboveground vegetation through the year. Standing aboveground biomass (live and senescent) in the spring of the following year (April 2022, 357 ± 148 g m^{-2}) was 39% lower than total aboveground biomass in November of 2021 (583 ± 208 g m^{-2}) (Fig 4b) and standing Hg pools were 32% lower in the subsequent spring (6.1 ± 1.9 µg m^{-2}) compared to peak fall levels (9.0 ± 3.3 µg m^{-2}) (Fig 4c), showing substantial losses of standing aboveground biomass and associated Hg pools over winter. Live root biomass in surface soils (top 20 cm) averaged 361 ± 114 g m^{-2} and live rhizome biomass were approximately twice as large (792 ± 231 g m^{-2}), for a combined live belowground biomass of $1,153\pm321$ g m^{-2} (Table S2). Belowground Hg pools associated with these live tissues averaged 70.0 ± 63.7 µg m^{-2} for roots, 38.1 ± 22.4 µg m^{-2} for rhizomes, and 108.1 ± 83.4 µg m^{-2} for the combined live belowground tissue, accounting for less than 0.5% of the total bulk soil Hg pool (Fig 5a, b, Table S2). We observed a much larger Hg pool associated with senesced biomass (roots, rhizomes, and detritus) averaging $4,116\pm1,141$ µg m^{-2}, accounting for 16.1% of the total bulk soil Hg pool. We estimated a total soil Hg pool in the top 40 cm using measured bulk densities (range of 0.22 and 0.37 g cm^{-3}) exceeding 25,000 µg m^{-2}, with most of this Hg associated with fine soil mineral and humus fraction (83.5%), while much smaller pools were contained in live and senesced plant tissues as mentioned above.

3.3 Hg stable isotope signatures to determine Hg sources

Live aboveground biomass showed negative mass-dependent fractionation (MDF) values for δ^{202}Hg between -1.61‰ and -1.07‰, and mass-independent (MIF) values were consistently positive with Δ^{199}Hg between 0.20‰ and 0.43‰ and Δ^{200}Hg values between 0.04‰ and 0.11‰ (Fig 6, Tables S3 and S6). These aboveground isotopic Hg signatures of salt marsh vegetation fell outside of the range commonly reported in foliar samples of terrestrial vegetation, both regarding mass-dependent and mass-independent signatures. Specifically, terrestrial vegetation Hg signatures are substantially more negative in δ^{202}Hg values (ranging from -3.06‰ to -2.37‰ [inter-quartile range, IQR, n = 120]) and both Δ^{199}Hg and Δ^{200}Hg values in terrestrial vegetation generally show negative values (Δ^{199}Hg: -0.42‰ to -0.27‰ IQR, Δ^{200}Hg: -0.05‰ to 0.01‰, IQR) (Fig 6, Table S6) (review by Zhou et al., 2021). Stable Hg isotope signatures of salt marsh plant roots were different from aboveground biomass, with less negative values for δ^{202}Hg (-0.75‰ and -0.66‰), less positive values for Δ^{199}Hg (0.11‰ and 0.22‰), and close to zero values (instead of positive values) for Δ^{200}Hg (-0.01‰ and 0.04‰) (Fig 6, Tables S3 and S6). The Hg isotope signatures of roots closely overlapped with signatures in surface marsh soils and deeper marsh soils (δ^{202}Hg: -0.92‰ to -0.29‰, Δ^{199}Hg: -0.09‰ to 0.20‰, and Δ^{200}Hg: -0.02‰ to 0.05‰, Tables S3 and S6). Similar to aboveground tissues, salt marsh soil isotopic Hg signatures were largely outside the ranges reported for upland soils, particularly for δ^{202}Hg values that are much more negative in upland soils (δ^{202}Hg generally between -0.5‰ and -2.9‰; review by Zhou et al., 2021). Hg isotope signatures of salt marsh rhizomes were highly variable and in-between values observed in foliage and soils. Specifically, rhizomes showed δ^{202}Hg values between -1.41‰ to -0.70‰, Δ^{199}Hg values between 0.13‰ to 0.22‰, and Δ^{200}Hg values between -0.05‰ to 0.04‰ (Fig 6, Tables S3 and S6).

4. Discussion

4.1 Salt marsh vegetation and soil Hg concentrations

Strong seasonal Hg concentration increases in salt marsh aboveground tissues were consistent with patterns reported from upland ecosystems, such as in forest foliage (Wohlgemuth et al., 2020). In upland systems, foliar Hg increases are attributed in large part

to atmospheric GEM uptake, which is taken up during the growing season by stomatal and non-stomatal (i.e., cuticular) leaf uptake (review by Zhou et al., 2021). Hg uptake is controlled by leaf physiological processes and related to photosynthetic capacity, leaf nitrogen concentrations, leaf mass area, and stomatal densities and conductance (Wohlgemuth et al., 2022). In support of a physiologically controlled Hg uptake process in salt marsh plants, we observed that Hg concentrations in senesced biomass in April of 2022 were not significantly enhanced compared to live biomass of the previous November (2021) (Fig 2), indicating that no significant Hg assimilation occurred during wintertime in senesced biomass. However, some increases in Hg concentrations occurred through November even after peak biomass was reached in August and September, which we attribute to continued active plant physiology through late season, as active photosynthesis was measured at least through October at this site (Forbrich et al., 2018; no data is available for November). In contrast to upland plant foliage, however, stable Hg isotope signatures of marsh aboveground biomass show distinctly different Hg source profiles indicating that Hg uptake was not dominated by atmospheric GEM uptake (see below).

Estimated daily Hg accumulation rates in *Sporobolus* -dominated aboveground biomass (0.08 µg kg^{-1} day^{-1}, Fig 2) was at the lower range of foliar accumulation rates reported in forest foliage (conifer needle: median of 0.07 µg kg^{-1} day^{-1}, deciduous leaf: median of 0.23 µg kg^{-1} day^{-1}; Wohlgemuth et al., 2022). This is consistent with the notion that low-statured grassland plants generally exhibit lower Hg concentrations (5 µg kg^{-1} [1-31 µg kg^{-1}]) than trees (e.g., forest foliage (20 µg kg^{-1} [2-62 µg kg^{-1}]) (review by Zhou et al., 2021), although it may also be due to different sources origins of Hg (section 4.2.1 below). Both dominant marsh species in this study also are C4 plants, which previous work shows have lower Hg concentrations compared to C3 species (e.g., 23±9 µg kg^{-1} versus 53±12 µg kg^{-1}, Canário et al., 2017). In a laboratory study with upland plants, suggested reasons for this was catalase activity, which is related to leaf uptake of Hg vapor and is about four times lower in C4 plants than C3 plants (Du and Fang, 1983).

Highest Hg concentrations in *S. alterniflorus* and *S. pumilus* were observed in fall (11.7 µg kg^{-1} and 24.0 µg kg^{-1}, respectively). Hg concentrations fell within concentration ranges reported from other uncontaminated marsh halophytes (Table S8) (Heller and Weber, 1998) (Kraus et al., 1986), but much lower than those from contaminated marshes (up to 90 µg kg^{-1}; (Windham et al., 2001) (Canário et al., 2017) (Wang et al., 2021).

In contrast to upland plants, salt marsh plants (including both *Sporobolus* species) have salt glands which are used for selective and active excretion of sea salt (Kirschner and Zinnert, 2020; Maricle et al., 2009). Salt glands have been linked to excretion of metals (Weis and Weis, 2004), and previous studies reported correlations between leaf surface Hg and sodium (Na) release in *S. alterniflorus* suggesting active Hg excretion by salt glands (Weis and Weis, 2004; Windham et al., 2001). Windham et al. (2001) proposed that in the Hackensack Meadowlands, a polluted salt marsh ecosystem, seasonal declines in Hg concentrations in *S. alternifla* leaves between May (90 µg kg^{-1}) to July (30 µg kg^{-1}) were driven by strong leaf excretion of Hg. By washing leaves of a number of samples, we found that washing removed about 6% of total leaf Hg in *S. alterniflorus* and 16% in *S. pumilus*, respectively (Table S7, note that we use the average wash-off fraction of 11% to estimate throughfall deposition in the mass balance estimation below). The relatively small loss of Hg associated with washing showed that most leaf Hg was structural and likely internal Hg, which along with observed seasonal Hg concentration increases does not support seasonal Hg losses nor seasonal concentration declines that were attributed to salt excretion by Windham et al.

Hg concentrations in live roots and rhizomes were much higher (11 and two times, respectively) than aboveground live biomass concentrations. This is consistent with previously reported data that reported high root Hg concentrations in salt marshes (Anjum et al., 2012; Cabrita et al., 2019; Canário et al., 2017; Garcia-Ordiales et al., 2020; Weis and Weis, 2004; Windham et al., 2003). We measured that Hg concentrations were higher in live roots of *S. pumilus* (258.9±70.3 µg kg^{-1}) than in *S. alterniflorus* (84.5±47.0 µg kg^{-1}) (Fig 3, Table S1). A possible reason for this is finer roots in *S. pumilus* (personal observation), and hence higher surface

262   to volume ratios, which may facilitate soil Hg uptake. In upland ecosystems, fine root Hg concentrations were reported to be higher

263   than in coarse roots as well (Wang et al., 2012; Wang et al., 2020). High root and rhizome Hg concentrations compared to

264   aboveground tissues in marsh plants contrast upland studies that generally report highest concentrations in foliage (20 µg kg kg⁻¹

265   [2–62 µg kg⁻¹]) and much lower concentrations in roots (7 µg kg⁻¹ [2–70 µg kg⁻¹]) (Zhou et al., 2021). An exception to this are

266   grassland systems that also report higher root Hg concentrations than in foliage, although the difference was much smaller (e.g.,

267   roots: 41±31 µg kg⁻¹; leaves: 20±10 µg kg⁻¹; (Zhou and Obrist, 2021)). Our data also showed generally much lower root Hg

268   concentrations in this marsh compared to contaminated sites (Anjum et al., 2012; Canário et al., 2017; Garcia-Ordiales et al., 2020)

269   (Wang et al., 2021) (Table S8). Overall, published studies suggest a large range of Hg concentrations in belowground salt marsh

270   biomass, which likely is due to different soil Hg concentrations as dominant Hg sources to roots (see section 4.2.1 below). The

271   higher concentrations of root and rhizomes in belowground tissues compared to aboveground biomass also suggests limited

272   translocation between belowground and aboveground tissues (Cavallini et al., 1999; Clemens and Ma, 2016; Graydon et al., 2009;

273   Wang et al., 2012).

4.2 Stable Hg isotope signatures and possible origins of Hg in salt marsh vegetation and soil

4.2.1 Salt marsh vegetation

276   One of the largest mass-dependent fractional (MDF) processes in the environmental systems is due to preferential uptake of light

277   atmospheric GEM isotopes by vegetation foliage that leads to large negative δ^{202}Hg signatures (generally below -2‰), while and

278   mass-independent signatures remain similar to that of atmospheric GEM (Demers et al., 2013; Enrico et al., 2016; Yu et al., 2016),

279   although a recent study also reported inconsistent MIF between foliage and the atmosphere (Wang et al., 2022). In terrestrial

280   ecosystems, studies have shown that the vegetation uptake of atmospheric GEM and subsequent litterfall, throughfall, and plant

281   senescence serves as the primary source of Hg loading (Demers et al., 2013; Jiskra et al., 2015; Louis et al., 2001; Obrist et al.,

282   2017; Wang et al., 2016; Zheng et al., 2016; Zhou et al., 2021). Aboveground tissues of salt marsh plants show a distinctly different

283   signature than upland foliage: specifically, MDF values were much less negative, and values of odd-MIF (Δ^{199}Hg) and even-MIF

284   (Δ^{200}Hg) were more positive compared to upland foliage (Fig 6, Table S6).

285   Hg signatures of salt marsh aboveground tissue were close to signatures of salt marsh soils, yet with slightly more negative δ^{202}Hg

286   values and more positive Δ^{199}Hg and Δ^{200}Hg values (Table S6). We used a ternary mixing model to identify potential Hg sources

287   and further quantify their contributions for salt marsh plant leaves based on MDF (δ^{202}Hg) and even-MIF (Δ^{200}Hg) (Demers et al.,

288   2013; Jiskra et al., 2017, 2021; Obrist et al., 2017). In our model, the dominant three end-member Hg sources include: (1) direct

289   uptake from marsh plant roots as represented by measured stable isotopes of roots, (2) atmospheric GEM uptake with typical

290   upland MDF reported in the literature, implemented using published date of upland foliage isotope data; and (3) precipitation Hg(II)

291   deposition obtained from published literature (see SI for details). Our best estimate shows that the Hg source in salt marsh

292   vegetation consists of a mixture of about 1/3 each from foliar uptake of atmospheric GEM uptake (about 32%), root uptake (about

293   35%), and precipitation deposition (about 33%). Note that these estimates assume that marsh foliage shows the same isotopic GEM

294   fractionation as upland foliage, and further assumes that translocation of root Hg has the same isotope patterns as measured in root

295   biomass. The percentage estimate derived from the tertiary mixing model shows substantial range of uncertainties (Figure S2) due

296   to a low number of samples and errors associated with analytical isotope determination. However, two different Monte Carlo

297   methods to estimate errors both suggest similar source contributions (i.e., about one third from each of the three endmembers).

298   Most notably, the biggest difference of marsh plants compared to upland plants is much less negative δ^{202}Hg values, suggesting

299   lower contributions from atmospheric GEM uptake which normally induces strong negative MDF in upland plants. Still, the

300   presence of atmospheric GEM uptake leads to δ^{202}Hg values in aboveground tissues that are more negative than in roots and soils.

Precipitation, which largely consists of oxidized Hg, shows a typical positive anomaly in $\Delta^{200}Hg$ linked to upper atmosphere GEM oxidation processes (Enrico et al., 2016; Jiskra et al., 2021; Zhou et al., 2021). Our results also suggest a more important role of root Hg transport to aboveground tissues in salt marsh vegetation (about one third) compared to upland ecosystems which normally reports root origins of less than 5% (review by Zhou et al., 2021). Previous salt marshes suggested inconsistent Hg source patterns: for example, an Hg isotope tracer study suggested minor root-to-leaf transport with soils accounting for a small percentage of Hg in marsh plants (i.e. 2.2-2.7% from Cabrita et al. (2019)), while a study based on bioaccumulation factors suggested a wide and inconstant range of soil Hg contribution to leaves (from 1.7-9.6 % to as high as 46%; Castro et al., 2009).

Roots of salt marsh plants show a Hg isotope signature that almost perfectly aligns with the signatures observed in soils, suggesting a dominant soil source. In terrestrial plants, Hg assimilated in belowground biomass also is considered largely of soil origin (Millhollen et al., 2006; Obrist et al., 2018; Zhou et al., 2021). This also has been proposed in aquatic plants (e.g., mangroves, sawgrass) where root Hg largely derives from surrounding soils (Huang et al., 2020; Mao et al., 2013; Yin et al., 2013). Finally, the few measured rhizome Hg isotope signatures indicate a mix of above-ground and belowground Hg sources, although rhizomes show a large variation in isotope signatures with some samples being closer to aboveground tissue and others being closer to root signatures. This observation would be consistent with the role of rhizomes as storage organs with over one year lifetime, whereby carbohydrates and nutrients are re-mobilized between rhizomes and above- and belowground organs based on plant allocation needs.

4.2.2 Salt marsh soil

The salt marsh soil isotope signature fell largely outside the range of soil Hg signatures reported from upland studies. In terrestrial environments, the strong MDF during foliar GEM uptake imprints a similar and typical terrestrial fingerprint on soil Hg, resulting in soil signatures with strong negative $\delta^{202}Hg$ and $\Delta^{200}Hg$ values similar to that of vegetation. Mixing models suggest upland soil Hg sources are dominated by atmospheric GEM (accounting for 53% to 92% of the source), which previously originated from plant Hg uptake and subsequent deposition (e.g., plant senescence) of overlying vegetation (Jiskra et al., 2018; Obrist et al., 2018; Zhou et al., 2021; Zhou and Obrist, 2021). These upland soil Hg isotope signatures propagate in watershed runoff (Jiskra, et al., 2017; Woerndle et al., 2018). Soils of our salt marsh study notably lacked the strong $\delta^{202}Hg$ depletion signal observed in uplands soils (e.g., $\delta^{202}Hg$ of marsh soils between -0.92‰ and -0.29‰, versus -0.5‰ to -2.5‰ in other soils, review by Zhou et al., 2021). This further supports that sources of Hg in marsh vegetation, which ultimately deposits to soils, are distinctly different from that of upland ecosystems. The isotopic signature of soil samples in Figure 6a also does not support that a simple two-way mixing of plant and precipitation Hg could explain salt marsh soils Hg signatures. Further terrestrial surface runoff, which generally shows typical terrestrial origin signatures (but was not measured in our study), also cannot explain marsh soil Hg isotope patterns. Seawater regularly floods the salt marsh during spring tides and storms and provide sediments for salt marsh soils (Millette et al., 2010). Recently reported ocean water Hg isotopes by Jiskra et al. (2021) show a strong overlap with Hg isotope signatures in salt marsh soil, whereby both $\Delta^{200}Hg$ and $\delta^{202}Hg$ fall between the ranges reported for seawater and ocean sediments (Fig S3). However, due to large variability in the data, we are unable to quantify potential source origins using a mixing model. However, the notion of potential ocean Hg sources would be consistent with a sediment mass balance study which showed that sediment loads in the Plum Island Sound estuary were dominated by imported ocean sediments (Hopkinson et al., 2018), with relatively minor import of sediments derived from the watershed. Finally, industrial and legacy contamination sources also may shape salt marsh soil Hg signatures. Generally, industrial Hg isotope signatures have been characterized by large ranges of negative $\delta^{202}Hg$ values and near-zero to positive $\Delta^{199}Hg$ and $\Delta^{200}Hg$ values (Fig S3, Table S6, see SI for details).

4.3 Hg mass balance and turnover fluxes associated with biomass dynamics.

4.3.1 Aboveground

We here estimate a mass balance of Hg sources and sinks associated with aboveground vegetation dynamics and turnover and compare these with previously reported fluxes such as lateral tidal exchanges, published wet and gaseous oxidized Hg, and particulate Hg deposition. Hg inputs to this salt marsh include wet Hg deposition, which based on interpolated data by the NADP program is estimated at 5.2 µg m^{-2} yr^{-1} (NADP, 2017), while a lower estimate of 2.9 µg m^{-2} yr^{-1} has been measured at a nearby coastal site on Cape Cod, Massachusetts (Engle et al., 2010). Combining these two data sets, we estimate a mid-point wet deposition of 4.1 µg m^{-2} yr^{-1}. Gaseous oxidized Hg (GOM) and particulate Hg (PHg) deposition in this area was estimated at 1.2 µg m^{-2} yr^{-1} based on measurements by Engle et al. (2010) and at 3.0 µg m^{-2} yr^{-1} at a deciduous forest (Harvard Forest) in Massachusetts (Obrist et al., 2021). Hence, a mid-point dry deposition of combined GOM and PHg is estimated at 2.1 µg m^{-2} yr^{-1} (Table 1, Fig 7). Aboveground vegetation Hg dynamics yields a total turnover of 9.0±3.3 µg m^{-2} yr^{-1} (combined live and senesced biomass at the end of the growing season), and isotope determination suggests that of this, about two thirds (represents an "external source" (5.9±2.1 µg m^{-2} yr^{-1}) derived from atmospheric GEM and precipitation uptake, while one third is from root uptake (3.1±1.1 µg m^{-2} yr^{-1}) and hence represents an internal plant-soil recycling within the ecosystem. ==Laboratory sample washing showed that in addition, on average about 11% of foliar Hg concentrations was subject to wash-off. In the absence of field throughfall measurements, we used this fraction to estimate throughfall deposition of Hg of 1.0±0.4 µg m^{-2} yr^{-1}, based on aboveground vegetation Hg pools (noting that this estimate is very preliminary).== Combined atmospheric Hg deposition attributable to aboveground vegetation hence is 6.9 µg m^{-2} yr^{-1}, and is close to the combined wet, GOM, and PHg deposition of 6.2 µg m^{-2} yr^{-1}. Combined atmospheric Hg sources in this system are estimated at 13.1 µg m^{-2} yr^{-1} (Table 1; a range of 7.7 to 19.5 µg m^{-2} yr^{-1}). Aboveground vegetation also results in lateral exchange of Hg between marsh and tidal water via wrack export, i.e., losses of plants and surface litter through tidal flushing. Although difficult to measure, wrack export in this area is composed primarily of *S. alterniflorus* plants (Hartman et al., 1983) and has been estimated to constitute 16-19% (mid-point of 17.5%) of accumulated biomass (Duarte, 2017; Duarte and Cebrián, 1996). Hence, we estimate that of the annual Hg uptake by aboveground biomass of 9.0 ±3.3 µg m^{-2} yr^{-1}, about 1.6 µg m^{-2} yr^{-1} (range of 1.4-1.7 µg Hg m^{-2} yr^{-1}) may be subject to wrack export. Scaling to the whole salt marsh area (==40 km^2==), the total wrack export from this marsh is estimated around 0.06 kg yr^{-1} (range of 0.06-0.07 kg yr^{-1}). In a previous study, we quantified Hg exports from the salt marsh system via tidal exchanges of dissolved and particulate Hg (without plants), and estimated 0.7 µg m^{-2} yr^{-1} of dissolved Hg export and 5.6 µg m^{-2} yr^{-1} of particulate Hg export from the marsh to the tidal water (Wang and Obrist, 2022). Our estimated annual Hg export by wrack is higher than lateral export of dissolved Hg, but much smaller than lateral export of particulate Hg. Duarte (2017) and Duarte and Cebrián (1996) estimated that about 27% of NPP is subject to herbivory (e.g., by ==marsh periwinkle and mummichog==), although another study estimated NPP loss due to herbivory at only 5% (Mann, 1988). Hence, an estimated 5% to 27% of plant Hg pools, or 0.5-2.4 µg Hg m^{-2} yr^{-1}, may be subject to herbivory. The largest fraction of NPP (57% to 80%), equivalent to 5.1-7.2 µg Hg m^{-2} yr^{-1}) likely remains in the system and is subject to net accumulation and decomposition. Considering all these inputs and outputs, we estimate a net present-day Hg mass accumulation in this salt marsh ecosystem between 0-11.5 µg m^{-2} yr^{-1} with a mid-point of 5.2 µg m^{-2} yr^{-1}, suggesting that this salt marsh currently represents a small net sink of environmental Hg. Absent of this estimate are gaseous exchange fluxes of GEM between soils/water surfaces and the atmosphere, which are currently being quantified using a tower-based measurement system (Edwards et al., 2005; Obrist et al., 2021).

4.3.2 Belowground

Many studies show that in salt marsh ecosystems, belowground productivity generally is equal or greater than aboveground biomass production, and this particularly applies for northern marshes (Blum, 1993; Morris, 2007; Tobias and Neubauer, 2019; Windham, 2001). Roots of both dominant species can grow to length of 8 to 20 cm (Blum, 1993; Muench and Elsey-Quirk, 2019). *S. alterniflorus* normally has large and thick rhizomes (normally ranging from 2-4 mm in diameter) with aerenchyma tissues to transport oxygen to submerged belowground tissue for respiration, while *S. pumilus* has relatively dense and fine roots with limited aerenchyma tissue which cannot support aerobic respiration when completely flooded (Muench and Elsey-Quirk, 2019). We measured live root biomass (upper 40 cm) of 444±87 g m^{-2} in *S. pumilus* and 278±61 g m^{-2} in *S. alterniflorus* cores (Table S1), which is consistent with reported denser root biomass in *S. pumilus* compared to *S. alterniflorus* (Muench and Elsey-Quirk, 2019). Combined live roots and rhizome biomass averaged 1,153±321 g m^{-2}, and thereby exceeded peak standing aboveground biomass of 830±415 g m^{-2} in August 2021.

Scaling up Hg pools using these belowground biomass data and measured Hg concentrations yields large belowground Hg pools. For example, the live belowground Hg pool (roots and rhizomes) is 108.1±83.4 µg m^{-2} and more than ten times larger than peak standing aboveground Hg pools (9.0±3.3 µg m^{-2}) (Fig 5a, Table S2). The Hg pool associated with senesced biomass (roots, rhizomes, and detritus) was over an order of magnitude larger (4,116±1,141 µg m^{-2}). Finally, the total pool of Hg in the top 40 cam of these marsh soils (all fractions) are estimated at >25,000 µg m^{-2}.

Turnover times of salt marsh macrophyte roots have been estimated at 0.6 yr^{-1} (0.2 to 1.9 yr^{-1}) (Ouyang et al., 2017) and 0.5 yr^{-1} (Blum, 1993), although longer turnover times have been proposed for creek-side plants (2.6 yr^{-1}, Blum, 1993). Assuming a belowground biomass turnover rate of 0.6 yr^{-1} (0.2 to 2.6 yr^{-1}), estimated Hg mass turnover associated with belowground biomass (root and rhizome) would be 58.6 µg m^{-2} yr^{-1} (19.5 to 253.8 µg m^{-2} yr^{-1}) (Table 1, Fig 7). Hence, belowground Hg turnover via plant tissues exceeds that of aboveground tissue (9.0±3.3 µg m^{-2} yr^{-1}) by a factor five, although it is largely unclear what the implications of this turnover may be. Given that the source of belowground tissue Hg is largely from soil uptake, large Hg belowground turnover flux does not likely provide an external source and instead represents an internal recycling of Hg between soils and belowground tissues. This recycling of Hg may have been various consequences, such as impacting mobility and bioavailability, phytostabilization by roots (Anjum et al., 2011), or remobilization of Hg associated with root decomposition. The estimated small net sink of environmental Hg in the above Hg mass balance is difficult to reconcile with the presence of very large soil Hg pools exceeding > 25,000 µg m^{-2}. It also is not consistent with the notion of this marsh as a hot spot of Hg pollution as reported from high blood Hg levels in predatory birds (Evers et al., 2007; Lane et al., 2020). It is possible that the current sink strength of Hg in this marsh is only a current snap shot in time, and that soil Hg in this marsh Hg largely have derived from historic legacy sources. Such potential sources may include imports of Hg or Hg-contaminated sediments from near-shore ocean into the Plum Island Sound, which in turn possibly may have originated from the nearby Merrimack River, a contaminated watershed from the long industrial history in New England.

5. Summary and conclusion

Measurements of Hg concentrations, fluxes, and turnover associated with vegetation in a salt marsh ecosystem with high above- and belowground NPP showed an annual Hg uptake in aboveground tissues of 9.0 ±3.3 µg m^{-2} yr^{-1}. Using a stable Hg isotope mixing model, we estimate that 35% of aboveground Hg originates from soil Hg uptake, 32% is from atmospheric GEM uptake, and 33% is from precipitation Hg(II) deposition. Estimated annual plant-derived atmospheric Hg deposition from plant senescence (i.e., litterfall) is estimated at 5.9±2.1 µg m^{-2} yr^{-1}, which is about half of that in forests where plant Hg assimilation of atmospheric

GEM is the dominant Hg source. We estimate an additional atmospheric Hg deposition by throughfall of 1.0 ± 0.4 µg m^{-2} yr^{-1}, for combined plant-derived Hg inputs of 6.9 µg m^{-2} yr^{-1}. This deposition is similar to combined wet and dry deposition of other atmospheric Hg forms. Seasonal and temporal Hg concentration and mass balance dynamics show strong seasonal increases during active growing season and a lack of concentration changes after senescence over winter, suggesting physiologically controlled uptake pathways. The presence of Hg within the aboveground tissues of salt marshes results in its direct release into tidal waters and oceans through the process of wrack deposition (tidal flushing of vegetation), contributing to an annual export of approximately 1.6 µg m^{-2} yr^{-1}). It also leads to herbivory uptake of Hg in a range of 0.5 to 2.4 µg Hg m^{-2} yr^{-1}, which may represent an internal recycling within the marsh system or possibly is subject to export (Table 1, Fig 7). The remainder of vegetation Hg is slowly incorporated into soils over winter and during the subsequent year. Overall, we estimate this marsh to presently serve as a small net Hg sink for environmental Hg of 5.2 µg m^{-2} yr^{-1}.

Belowground Hg pools associated with live tissues (108.1 ± 83.4 µg m^{-2}) were over ten times larger than peak aboveground Hg pools and resulted in a substantial annual Hg turnover flux of 58.6 µg m^{-2} yr^{-1}. The source of root Hg is likely from soil uptake, while belowground rhizomes show variable sources both from aboveground and root tissues. Turnover of Hg associated with belowground tissues largely reflects internal recycling between soils and plants, with poorly understood impacts on Hg partitioning, bioavailability, and mobility. Hg associated with roots and rhizomes only accounted for about 0.4% of total belowground Hg pools, with the largest soil Hg pools associated with fine soil mineral and humus fractions (83.5%).

6. Acknowledgements

We thank Keely O'Beirne, Madison Sachs, and Silas Bollen for help with vegetation sampling and laboratory analysis of initial plant and soil mercury samples. We thank Nancy Pau and the Parker River National Wildlife Refuge for sampling permits and acces. We thank Samuel Kelsey, Anne Giblin and other researchers from the Plum Island Ecosystem Long-Term Ecological Research project for support and information about the estuary. Funding was provided by an award from the U.S. National Science Foundation Division of Environmental Biology (Award Number: 2027038).

Code and data availability

Upon request, the original data supporting the conclusions of this study can be provided.

Author contribution

DO and TW designed and carried out the study; TW, BYD, JZ, and JP contributed to samples collection; TW, BYD, JP, PB conducted samples analysis; TW, BYD, IF, EM, PB, and DO contributed to interpreting the data and figures; TW, IF, JZ, ES, BP, CC, and DO contributed to writing and editing the manuscript. All authors contributed to the review of the manuscript. DO and IF secured funding for the project.

Competing interests

The contact author has declared that none of the authors has any competing interests.

445 **Reference**

446 Amos, H. M., Jacob, D. J., Kocman, D., Horowitz, H. M., Zhang, Y., Dutkiewicz, S., Horvat, M., Corbitt, E. S., Krabbenhoft, D.
447   P., & Sunderland, E. M. (2014). Global biogeochemical implications of mercury discharges from rivers and sediment
448   burial. *Environmental Science and Technology*, *48*(16), 9514–9522. https://doi.org/10.1021/es502134t

449 Anjum, N. A., Ahmad, I., Válega, M., Pacheco, M., Figueira, E., Duarte, A. C., & Pereira, E. (2011). Impact of seasonal
450   fluctuations on the sediment-mercury, its accumulation and partitioning in Halimione portulacoides and Juncus maritimus
451   collected from Ria de Aveiro coastal lagoon (Portugal). *Water, Air, and Soil Pollution*, *222*(1–4), 1–15.
452   https://doi.org/10.1007/s11270-011-0799-4

453 Anjum, N. A., Ahmad, I., Válega, M., Pacheco, M., Figueira, E., Duarte, A. C., Pereira, E., Anjum, N. A., Ahmad, I., Válega, :
454   M, Duarte, A. C., Pereira, E., Pacheco, M., & Figueira, E. (2012). Salt marsh macrophyte Phragmites australis strategies
455   assessment for its dominance in mercury-contaminated coastal lagoon (Ria de Aveiro, Portugal). *Environ Sci Pollut Res*,
456   *19*, 2879–2888. https://doi.org/10.1007/s11356-012-0794-3

457 Arp, W. J., Drake, B. G., Pockman, W. T., Curtis, P. S., & Whigham, D. F. (1993). Manual of the Vascular Flora of the
458   Carolinas. *Vegetatio*, *104*(105), 133–143. https://doi.org/20029742

459 Bertness, M. D. (1991). Zonation of Spartina patens and Spartina alterniflora in a New England salt marsh. *Ecology*, *72*(1), 138–
460   148. https://doi.org/10.2307/1938909

461 Blum, J. D., & Bergquist, B. A. (2007). Reporting of variations in the natural isotopic composition of mercury. *Analytical and*
462   *Bioanalytical Chemistry*, *388*(2), 353–359. https://doi.org/10.1007/s00216-007-1236-9

463 Blum, J. D., & Johnson, M. W. (2017). Recent developments in mercury stable isotope analysis. *Reviews in Mineralogy and*
464   *Geochemistry*, *82*(July 2013), 733–757. https://doi.org/10.2138/rmg.2017.82.17

465 Blum, L. K. (1993). Spartina alterniflora root dynamics in a Virginia marsh. *Marine Ecology Progress Series*, *102*, 169–178.

466 Cabrita, M. T., Duarte, B., Cesário, R., Mendes, R., Hintelmann, H., Eckey, K., Dimock, B., Caçador, I., & Canário, J. (2019).
467   Mercury mobility and effects in the salt-marsh plant Halimione portulacoides: Uptake, transport, and toxicity and tolerance
468   mechanisms. *Science of The Total Environment*, *650*, 111–120. https://doi.org/10.1016/j.scitotenv.2018.08.335

469 Canário, J., Poissant, L., Pilote, M., Caetano, M., Hintelmann, H., & O'Driscoll, N. J. (2017). Salt-marsh plants as potential
470   sources of Hg0 into the atmosphere. *Atmospheric Environment*, *152*, 458–464.
471   https://doi.org/10.1016/j.atmosenv.2017.01.011

472 Castro, R., Pereira, S., Lima, A., Corticeiro, S., Válega, M., Pereira, E., Duarte, A., & Figueira, E. (2009). Accumulation,
473   distribution and cellular partitioning of mercury in several halophytes of a contaminated salt marsh. *Chemosphere*, *76*(10),
474   1348–1355. https://doi.org/10.1016/j.chemosphere.2009.06.033

475 Cavallini, A., Natali, L., Durante, M., & Maserti, B. (1999). Mercury uptake, distribution and DNA affinity in durum wheat
476   (Triticum durum Desf.) plants. *Science of the Total Environment*, *243–244*, 119–127. https://doi.org/10.1016/S0048-
477   9697(99)00367-8

478 Cheng, X., Luo, Y., Chen, J., Lin, G., Chen, J., & Li, B. (2006). Short-term C4 plant Spartina alterniflora invasions change the
479   soil carbon in C3 plant-dominated tidal wetlands on a growing estuarine Island. *Soil Biology and Biochemistry*, *38*(12),
480   3380–3386. https://doi.org/10.1016/j.soilbio.2006.05.016

481 Clemens, S., & Ma, J. F. (2016). Toxic Heavy Metal and Metalloid Accumulation in Crop Plants and Foods. *Annual Review of*
482   *Plant Biology*, *67*, 489–512. https://doi.org/10.1146/annurev-arplant-043015-112301

483 Curtis, P. S., Balduman, L. M., Drake, B. G., & Whigham, D. F. (1990). Elevated Atmospheric CO2 Effects on Belowground
484   Processes in C3 and C4 Estuarine Marsh Communities. *Source: Ecology*, *71*(5), 2001–2006.

485   Demers, J. D., Blum, J. D., & Zak, D. R. (2013). Mercury isotopes in a forested ecosystem: Implications for air-surface exchange
486   dynamics and the global mercury cycle. *Global Biogeochemical Cycles*, *27*(1), 222–238. https://doi.org/10.1002/gbc.20021
487   Du, S., & Fang, S. C. (1983). Catalase activity of C3 and C4 species and its relationship to mercury vapor uptake. *Environmental*
488   *and Experimental Botany*, *23*(4), 347–353. https://doi.org/10.1016/0098-8472(83)90009-6
489   Duarte, C. M. (2017). Reviews and syntheses: Hidden forests, the role of vegetated coastal habitats in the ocean carbon budget.
490   *Biogeosciences*, *14*(2), 301–310. https://doi.org/10.5194/bg-14-301-2017
491   Duarte, C. M., & Cebrián, J. (1996). The fate of marine autotrophic production. *Limnology and Oceanography*, *41*(8), 1758–
492   1766. https://doi.org/10.4319/LO.1996.41.8.1758
493   Edwards, G. C., Rasmussen, P. E., Schroeder, W. H., Wallace, D. M., Halfpenny-Mitchell, L., Dias, G. M., Kemp, R. J., &
494   Ausma, S. (2005). Development and evaluation of a sampling system to determine gaseous Mercury fluxes using an
495   aerodynamic micrometeorological gradient method. *Journal of Geophysical Research D: Atmospheres*, *110*(10), 1–11.
496   https://doi.org/10.1029/2004JD005187
497   Elsey-Quirk, T., Seliskar, D. M., & Gallagher, J. L. (2011). Nitrogen Pools of Macrophyte Species in a Coastal Lagoon Salt
498   Marsh: Implications for Seasonal Storage and Dispersal. *Estuaries and Coasts*, *34*(3), 470–482.
499   https://doi.org/10.1007/s12237-011-9379-5
500   Engle, M. A., Tate, M. T., Krabbenhoft, D. P., Schauer, J. J., Kolker, A., Shanley, J. B., & Bothner, M. H. (2010). Comparison of
501   atmospheric mercury speciation and deposition at nine sites across central and eastern North America. *Journal of*
502   *Geophysical Research Atmospheres*, *115*(18). https://doi.org/10.1029/2010JD014064
503   Enrico, M., Balcom, P., Johnston, D. T., Foriel, J., & Sunderland, E. M. (2021). Simultaneous combustion preparation for
504   mercury isotope analysis and detection of total mercury using a direct mercury analyzer. *Analytica Chimica Acta*, *1154*.
505   https://doi.org/10.1016/j.aca.2021.338327
506   Enrico, M., Roux, G. Le, Marusczak, N., Heimbürger, L. E., Claustres, A., Fu, X., Sun, R., & Sonke, J. E. (2016). Atmospheric
507   Mercury Transfer to Peat Bogs Dominated by Gaseous Elemental Mercury Dry Deposition. *Environmental Science and*
508   *Technology*, *50*(5), 2405–2412. https://doi.org/10.1021/acs.est.5b06058
509   Evers, D. C., Han, Y.-J., Driscoll, C. T., Kamman, N. C., Goodale, M. W., Lambert, K. F., Holsen, T. M., Chen, C. Y., Clair, T.
510   A., & Butler, T. (2007). Biological Mercury Hotspots in the Northeastern United States and Southeastern Canada.
511   *BioScience*, *57*(1), 29–43. https://doi.org/10.1641/b570107
512   Fisher, L. S., & Wolfe, M. H. (2012). Examination of mercury inputs by throughfall and litterfall in the Great Smoky Mountains
513   National Park. *Atmospheric Environment*, *47*, 554–559. https://doi.org/10.1016/j.atmosenv.2011.10.017
514   Forbrich, I., Giblin, A. E., & Hopkinson, C. S. (2018). Constraining Marsh Carbon Budgets Using Long-Term C Burial and
515   Contemporary Atmospheric CO2 Fluxes. *Journal of Geophysical Research: Biogeosciences*, *123*(3), 867–878.
516   https://doi.org/10.1002/2017JG004336
517   Fu, X., Zhang, H., Liu, C., Zhang, H., Lin, C. J., & Feng, X. (2019). Significant Seasonal Variations in Isotopic Composition of
518   Atmospheric Total Gaseous Mercury at Forest Sites in China Caused by Vegetation and Mercury Sources. *Environmental*
519   *Science and Technology*, *53*(23), 13748–13756. https://doi.org/10.1021/acs.est.9b05016
520   Garcia-Ordiales, E., Roqueñí, N., & Loredo, J. (2020). Mercury bioaccumulation by Juncus maritimus grown in a Hg
521   contaminated salt marsh (northern Spain). *Marine Chemistry*, *226*, 103859.
522   https://doi.org/10.1016/j.marchem.2020.103859
523   Graydon, J. A., St. Louis, V. L., Hintelmann, H., Lindberg, S. E., Sandilands, K. A., Rudd, J. W. M., Kelly, C. A., Tate, M. T.,
524   Krabbenhoft, D. P., & Lehnherr, I. (2009). Investigation of uptake and retention of atmospheric Hg(II) by boreal forest

525   plants using stable Hg isotopes. *Environmental Science and Technology*, *43*(13), 4960–4966.

526   https://doi.org/10.1021/es900357s

527   Grigal, D. F. (2003). Mercury Sequestration in Forests and Peatlands. *Journal of Environmental Quality*, *32*(2), 393–405.

528   https://doi.org/10.2134/jeq2003.3930

529   Grigal, D. F., Kolka, R. K., Fleck, J. A., & Nater, E. A. (2000). Mercury budget of an upland-peatland watershed.

530   *Biogeochemistry*, *50*(1), 95–109. https://doi.org/10.1023/A:1006322705566

531   Hartman, J., Caswell, H., & Valiela, I. (1983). Effects of wrack accumulation on salt marsh vegetation. *Oceanologica Acta*,

532   *Actes 17e*(February), 99–102.

533   He, L., Chen, J. M., Pan, Y., Birdsey, R., & Kattge, J. (2012). Relationships between net primary productivity and forest stand

534   age in U.S. forests. *Global Biogeochemical Cycles*, *26*(3). https://doi.org/10.1029/2010GB003942

535   Heller, A. A., & Weber, J. H. (1998). Seasonal study of speciation of mercury(II) and monomethylmercury in Spartina

536   alterniflora from the Great Bay Estuary, NH. *Science of the Total Environment*, *221*(2–3), 181–188.

537   https://doi.org/10.1016/S0048-9697(98)00285-X

538   Hopkinson, C. S., Morris, J. T., Fagherazzi, S., Wollheim, W. M., & Raymond, P. A. (2018). Lateral Marsh Edge Erosion as a

539   Source of Sediments for Vertical Marsh Accretion. *Journal of Geophysical Research: Biogeosciences*, *123*(8), 2444–2465.

540   https://doi.org/10.1029/2017JG004358

541   Huang, S., Jiang, R., Song, Q., Zhang, Y., Huang, Q., Su, B., Chen, Y., Huo, Y., & Lin, H. (2020). Study of mercury transport

542   and transformation in mangrove forests using stable mercury isotopes. *Science of the Total Environment*, *704*, 135928.

543   https://doi.org/10.1016/j.scitotenv.2019.135928

544   Iverfeldt, Å. (1991). Mercury in forest canopy throughfall water and its relation to atmospheric deposition. *Water Air & Soil*

545   *Pollution*, *56*(1), 553–564. https://doi.org/10.1007/BF00342299

546   Jackson, A. K., Evers, D. C., Etterson, M. A., Condon, A. M., Folsom, S. B., Detweiler, J., Schmerfeld, J., & Cristol, D. A.

547   (2011). Mercury Exposure Affects The Reproductive Success of a Free-living Terrestrial Songbird, the Carolina Wren

548   (Thryothorus Ludovicianus). In *The Auk* (Vol. 128, Issue 4). https://doi.org/10.1525/auk.2011.11106

549   Jiskra, M., Heimbürger-Boavida, L.-E., Desgranges, M.-M., Petrova, M. V., Dufour, A., Ferreira-Araujo, B., Masbou, J.,

550   Chmeleff, J., Thyssen, M., Point, D., & Sonke, J. E. (2021). Mercury stable isotopes constrain atmospheric sources to the

551   ocean. *Nature*, *597*(7878), 678–682. https://doi.org/10.1038/s41586-021-03859-8

552   Jiskra, M., Sonke, J. E., Obrist, D., Bieser, J., Ebinghaus, R., Myhre, C. L., Pfaffhuber, K. A., Wängberg, I., Kyllönen, K.,

553   Worthy, D., Martin, L. G., Labuschagne, C., Mkololo, T., Ramonet, M., Magand, O., & Dommergue, A. (2018). A

554   vegetation control on seasonal variations in global atmospheric mercury concentrations. *Nature Geoscience*, *11*(4), 244–

555   250. https://doi.org/10.1038/s41561-018-0078-8

556   Jiskra, M., Wiederhold, J. G., Skyllberg, U., Kronberg, R. M., Hajdas, I., & Kretzschmar, R. (2015). Mercury Deposition and

557   Re-emission Pathways in Boreal Forest Soils Investigated with Hg Isotope Signatures. *Environmental Science and*

558   *Technology*, *49*(12), 7188–7196. https://doi.org/10.1021/acs.est.5b00742

559   Jiskra, M., Wiederhold, J. G., Skyllberg, U., Kronberg, R. M., & Kretzschmar, R. (2017). Source tracing of natural organic

560   matter bound mercury in boreal forest runoff with mercury stable isotopes. *Environmental Science: Processes and Impacts*,

561   *19*(10), 1235–1248. https://doi.org/10.1039/c7em00245a

562   Kirschner, A. S., & Zinnert, J. C. (2020). Two low-lying coastal grassland species differ in mechanistic response to saline

563   flooding stress. *Plant Ecology*, *221*(6), 475–485. https://doi.org/10.1007/s11258-020-01026-z

564   Kraus, M. L., Weis, P., & Crow, J. H. (1986). The excretion of heavy metals by the salt marsh cord grass,Spartina alterniflora,

565   and Spartina's role in mercury cycling. *Marine Environmental Research*, *20*(4), 307–316. https://doi.org/10.1016/0141-
566   1136(86)90056-5

567   Lane, O., Adams, E. M., Pau, N., O'Brien, K. M., Regan, K., Farina, M., Schneider-Moran, T., & Zarudsky, J. (2020). Long-
568   term monitoring of mercury in adult saltmarsh sparrows breeding in Maine, Massachusetts and New York, USA 2000–
569   2017. In *Ecotoxicology* (Vol. 29, Issue 8). Springer US. https://doi.org/10.1007/s10646-020-02180-w

570   Lane, O. P., O'Brien, K. M., Evers, D. C., Hodgman, T. P., Major, A., Pau, N., Ducey, M. J., Taylor, R., & Perry, D.
571   (2011). Mercury in breeding saltmarsh sparrows (Ammodramus caudacutus caudacutus). *Ecotoxicology*, *20*(8), 1984–
572   1991. https://doi.org/10.1007/s10646-011-0740-z

573   Liu, M., Zhang, Q., Maavara, T., Liu, S., Wang, X., & Raymond, P. A. (2021). Rivers as the largest source of mercury to coastal
574   oceans worldwide. *Nature Geoscience*, *14*(9), 672–677. https://doi.org/10.1038/s41561-021-00793-2

575   Louis, V. L. S. T., Rudd, J. W. M., Kelly, C. A., Hall, B. D., Rolfhus, K. R., Scott, K. J., Lindberg, S. E., & Dong, W. (2001).
576   Importance of the forest canopy to fluxes of methyl mercury and total mercury to boreal ecosystems. *Environmental*
577   *Science and Technology*, *35*(15), 3089–3098. https://doi.org/10.1021/es001924p

578   Mann, K. H. (1988). Production and use of detritus in various freshwater, estuarine, and coastal marine ecosystems. *Limnology*
579   *and Oceanography*, *33*(4part2), 910–930. https://doi.org/10.4319/LO.1988.33.4PART2.0910

580   Mao, Y., Li, Y., Richards, J., & Cai, Y. (2013). Investigating uptake and translocation of mercury species by sawgrass (Cladium
581   jamaicense) using a stable isotope tracer technique. *Environmental Science and Technology*, *47*(17), 9678–9684.
582   https://doi.org/10.1021/es400546s

583   Maricle, B. R., Koteyeva, N. K., Voznesenskaya, E. V., Thomasson, J. R., & Edwards, G. E. (2009). Diversity in leaf anatomy,
584   and stomatal distribution and conductance, between salt marsh and freshwater species in the C4 genus Spartina (Poaceae).
585   *New Phytologist*, *184*(1), 216–233. https://doi.org/10.1111/J.1469-8137.2009.02903.X

586   Marques, B., Lillebø, A. I., Pereira, E., & Duarte, A. C. (2011). Mercury cycling and sequestration in salt marshes sediments: An
587   ecosystem service provided by Juncus maritimus and Scirpus maritimus. *Environmental Pollution*, *159*(7), 1869–1876.
588   https://doi.org/10.1016/j.envpol.2011.03.036

589   Millette, T. L., Argow, B. A., Marcano, E., Hayward, C., Hopkinson, C. S., & Valentine, V. (2010). Salt Marsh
590   Geomorphological Analyses via Integration of Multitemporal Multispectral Remote Sensing with LIDAR and GIS .
591   *Journal of Coastal Research*, *265*, 809–816. https://doi.org/10.2112/jcoastres-d-09-00101.1

592   Millhollen, A. G., Gustin, M. S., & Obrist, D. (2006). Foliar Mercury Accumulation and Exchange for Three Tree Species.
593   *Environmental Science & Technology*, *40*(19), 6001–6006. https://doi.org/10.1021/es0609194

594   Morris, J. T. (2007). Estimating Net Primary Production of Salt Marsh Macrophytes. In *Principles and Standards for Measuring*
595   *Primary Production* (Vol. 15, Issue 1, pp. 106–119). Oxford University Press.
596   https://doi.org/10.1093/acprof:oso/9780195168662.003.0007

597   Morris, J. T., Sundberg, K., & Hopkinson, C. S. (2013). Salt marsh primary production and its responses to relative sea level and
598   nutrientsin estuaries at plum island, Massachusetts, and North Inlet, South Carolina, USA. *Oceanography*, *26*(3), 78–84.
599   https://doi.org/10.5670/oceanog.2013.48

600   Muench, A., & Elsey-Quirk, T. (2019). Competitive reversal between plant species is driven by species-specific tolerance to
601   flooding stress and nutrient acquisition during early marsh succession. *J Appl Ecol*, *56*, 2236–2247.
602   https://doi.org/10.1111/1365-2664.13458

603   NADP. (2017). *National Atmospheric Deposition Program, Mercury Deposition Network*.
604   http://nadp.slh.wisc.edu/maplib/pdf/mdn/hg_Conc_2017.pdf

605   Niu, Z., Zhang, X., Wang, Z., & Ci, Z. (2011). Field controlled experiments of mercury accumulation in crops from air and soil.

606   *Environmental Pollution*, *159*(10), 2684–2689. https://doi.org/10.1016/j.envpol.2011.05.029

607   NOAA. (2020). *National Oceanic and Atmospheric Administration Tide Predictions*.

608   https://www.tidesandcurrents.noaa.gov/noaatidepredictions.html?id=8441241

609   Obrist, D., Agnan, Y., Jiskra, M., Olson, C. L., Colegrove, D. P., Hueber, J., Moore, C. W., Sonke, J. E., & Helmig, D. (2017).

610   Tundra uptake of atmospheric elemental mercury drives Arctic mercury pollution. *Nature*, *547*(7662), 201–204.

611   https://doi.org/10.1038/nature22997

612   Obrist, D., Kirk, J. L., Zhang, L., Sunderland, E. M., Jiskra, M., & Selin, N. E. (2018). A review of global environmental

613   mercury processes in response to human and natural perturbations: Changes of emissions, climate, and land use. *Ambio*,

614   *47*(2), 116–140. https://doi.org/10.1007/s13280-017-1004-9

615   Obrist, D., Roy, E. M., Harrison, J. L., Kwong, C. F., William Munger, J., Moosmüller, H., Romero, C. D., Sun, S., Zhou, J., &

616   Commane, R. (2021). Previously unaccounted atmospheric mercury deposition in a midlatitude deciduous forest.

617   *Proceedings of the National Academy of Sciences of the United States of America*, *118*(29).

618   https://doi.org/10.1073/pnas.2105477118

619   Ouyang, X., Lee, S. Y., & Connolly, R. M. (2017). The role of root decomposition in global mangrove and saltmarsh carbon

620   budgets. In *Earth-Science Reviews* (Vol. 166, pp. 53–63). https://doi.org/10.1016/j.earscirev.2017.01.004

621   Raymond, P. A., & Hopkinson, C. S. (2003). Ecosystem Modulation of Dissolved Carbon Age in a Temperate Marsh-Dominated

622   Estuary. *Ecosystems*, *6*(7), 694–705. https://doi.org/10.1007/s10021-002-0213-6

623   Rea, A. W., Keeler, G. J., & Scherbatskoy, T. (1996). The deposition of mercury in throughfall and litterfall in the Lake

624   Champlain watershed: A short-term study. *Atmospheric Environment*, *30*(19), 3257–3263. https://doi.org/10.1016/1352-

625   2310(96)00087-8

626   Sun, L., Shao, D., Xie, T., Gao, W., Ma, X., Ning, Z., & Cui, B. (2020). How does Spartina alterniflora invade in salt marsh in

627   relation to tidal channel networks? Patterns and processes. *Remote Sensing*, *12*(18). https://doi.org/10.3390/RS12182983

628   Tobias, C., & Neubauer, S. (2009). Salt Marsh Biogeochemistry - An Overview. In G. M. E. Perillo, E. Wolanski, D. R. Cahoon,

629   & M. M. Brinson (Eds.), *Coastal Wetlands: An Integrated Ecosystem Approach* (pp. 1–57). Elsevier.

630   Tobias, Craig, & Neubauer, S. C. (2019). Salt Marsh Biogeochemistry—An Overview. *Coastal Wetlands: An Integrated*

631   *Ecosystem Approach*, 539–596. https://doi.org/10.1016/B978-0-444-63893-9.00016-2

632   U.S. EPA. (1998). Method 7473, Mercury in solids and solutions by thermal decomposition, amalgamation, and atomic

633   absorption spectrophotometry. In *Revision 0. Washington, DC*.

634   Valiela, I., Teal, J. M., & Persson, N. Y. (1976). Production and dynamics of experimentally enriched salt marsh vegetation:

635   Belowground biomass. *Limnology and Oceanography*, *21*(2), 245–252. https://doi.org/10.4319/lo.1976.21.2.0245

636   Visser, J. M., Midway, S., Baltz, D. M., & Sasser, C. E. (2018). Ecosystem structure of tidal saline marshes. In *Coastal*

637   *Wetlands: An Integrated Ecosystem Approach* (pp. 519–538). Elsevier. https://doi.org/10.1016/B978-0-444-63893-

638   9.00015-0

639   Wang, J. J., Guo, Y. Y., Guo, D. L., Yin, S. L., Kong, D. L., Liu, Y. S., & Zeng, H. (2012). Fine root mercury heterogeneity:

640   Metabolism of lower-order roots as an effective route for mercury removal. *Environmental Science and Technology*, *46*(2),

641   769–777. https://doi.org/10.1021/es2018708

642   Wang, T., & Obrist, D. (2022). Inorganic and methylated mercury dynamics in estuarine water of a salt marsh in Massachusetts,

643   USA. *Environmental Pollution*, *294*. https://doi.org/10.1016/j.envpol.2021.118657

644   Wang, X., Bao, Z., Lin, C. J., Yuan, W., & Feng, X. (2016). Assessment of Global Mercury Deposition through Litterfall.

645   *Environmental Science and Technology*, *50*(16), 8548–8557. https://doi.org/10.1021/acs.est.5b06351

646 Wang, X., Yuan, W., Lin, C.-J., & Feng, X. (2022). Mercury cycling and isotopic fractionation in global forests. *Critical*

647   *Reviews in Environmental Science and Technology*, *52*(21), 3763–3786. https://doi.org/10.1080/10643389.2021.1961505

648 Wang, X., Yuan, W., Lin, C.-J., Zhang, L., Zhang, H., & Feng, X. (2019). Climate and Vegetation As Primary Drivers for Global

649   Mercury Storage in Surface Soil. *Environmental Science & Technology*, *53*(18), 10665–10675.

650   https://doi.org/10.1021/acs.est.9b02386

651 Wang, X., Yuan, W., Lin, C. J., Luo, J., Wang, F., Feng, X., Fu, X., & Liu, C. (2020). Underestimated Sink of Atmospheric

652   Mercury in a Deglaciated Forest Chronosequence. *Environmental Science and Technology*, *54*(13), 8083–8093.

653   https://doi.org/10.1021/acs.est.0c01667

654 Wang, X., Yuan, W., Lin, C. J., Wang, D., Luo, J., Xia, J., Zhang, W., Wang, F., & Feng, X. (2022). Root uptake dominates

655   mercury accumulation in permafrost plants of Qinghai-Tibet Plateau. *Communications Earth and Environment*, *3*(1), 1–10.

656   https://doi.org/10.1038/s43247-022-00619-y

657 Wang, Y., Wang, Z., Zheng, X., & Zhou, L. (2021). Influence of Spartina alterniflora invasion on mercury storage and

658   methylation in the sediments of Yangtze River estuarine wetlands. *Estuarine, Coastal and Shelf Science*, *265*(June 2021),

659   107717. https://doi.org/10.1016/j.ecss.2021.107717

660 Weis, J. S., & Weis, P. (2004). Metal uptake, transport and release by wetland plants: implications for phytoremediation and

661   restoration. *Environment International*, *30*(5), 685–700. https://doi.org/10.1016/j.envint.2003.11.002

662 Wilson, C. A., Hughes, Z. J., FitzGerald, D. M., Hopkinson, C. S., Valentine, V., & Kolker, A. S. (2014). Saltmarsh pool and

663   tidal creek morphodynamics: Dynamic equilibrium of northern latitude saltmarshes? *Geomorphology*, *213*, 99–115.

664   https://doi.org/10.1016/j.geomorph.2014.01.002

665 Windham, L, Weis, J. ., & Weis, P. (2003). Uptake and distribution of metals in two dominant salt marsh macrophytes, Spartina

666   alterniflora (cordgrass) and Phragmites australis (common reed). *Estuarine, Coastal and Shelf Science*, *56*(1), 63–72.

667   https://doi.org/10.1016/S0272-7714(02)00121-X

668 Windham, Lisamarie. (2001). Comparison of biomass production and decomposition between Phragmites australis (common

669   reed) and spartina patens (salt hay grass) in brackish tidal marshes of New Jersey, USA. *Wetlands*, *21*(2), 179–188.

670   https://doi.org/10.1672/0277-5212(2001)021[0179:COBPAD]2.0.CO;2

671 Windham, Lisamarie, Wei, J. S., & Weis, P. (2001). *Patterns and Processes of Mercury Release from Leaves of Two Dominant*

672   *Salt Marsh Macrophytes , Phragmites australis and Spartina alterniflora*. *24*(6), 787–795.

673   https://doi.org/https://doi.org/10.2307/1353170

674 Windham, Lisamarie, Weis, J. S., & Weis, P. (2001). Patterns and processes of mercury release from leaves of two dominant salt

675   marsh macrophytes, Phragmites australis and Spartina alterniflora. *Estuaries*, *24*(6 A), 787–795.

676   https://doi.org/10.2307/1353170

677 Windham, Lisamarie, Weis, J. S., Weis, P., Wei, J. S., Weis, P., Weis, J. S., & Weis, P. (2001). Patterns and Processes of

678   Mercury Release from Leaves of Two Dominant Salt Marsh Macrophytes , Phragmites australis and Spartina alterniflora.

679   *Estuaries*, *24*(6), 787–795. https://doi.org/https://doi.org/10.2307/1353170

680 Woerndle, G. E., Tsz-Ki Tsui, M., Sebestyen, S. D., Blum, J. D., Nie, X., & Kolka, R. K. (2018). New Insights on Ecosystem

681   Mercury Cycling Revealed by Stable Isotopes of Mercury in Water Flowing from a Headwater Peatland Catchment.

682   *Environmental Science and Technology*, *52*(4), 1854–1861. https://doi.org/10.1021/acs.est.7b04449

683 Wohlgemuth, L., Osterwalder, S., Joseph, C., Kahmen, A., Hoch, G., Alewell, C., & Jiskra, M. (2020). A bottom-up

684   quantification of foliar mercury uptake fluxes across Europe. *Biogeosciences*, *17*(24), 6441–6456.

685   https://doi.org/10.5194/bg-17-6441-2020

686 Wohlgemuth, L., Rautio, P., Ahrends, B., Russ, A., Vesterdal, L., Waldner, P., Timmermann, V., Eickenscheidt, N., Fürst, A.,

687   Greve, M., Roskams, P., Thimonier, A., Nicolas, M., Kowalska, A., Ingerslev, M., Merilä, P., Benham, S., Iacoban, C.,

688   Hoch, G., … Jiskra, M. (2022). Physiological and climate controls on foliar mercury uptake by European tree species.

689   *Biogeosciences*, *19*, 1335–1353. https://doi.org/10.5194/bg-19-1335-2022

690 Wolanski, E., Perillo, G. M. E., Brinson, M. M., & Cahoon, D. R. (2009). *Coastal Wetlands: A Synthesis*. Elsevier. Amsterdam,

691   Países Bajos. http://www.elsevier.com

692 Yin, R., Feng, X., & Meng, B. (2013). Stable mercury isotope variation in rice plants (Oryza sativa L.) from the Wanshan

693   mercury Mining District, SW China. *Environmental Science and Technology*, *47*(5), 2238–2245.

694   https://doi.org/10.1021/es304302a

695 Yu, B., Fu, X., Yin, R., Zhang, H., Wang, X., Lin, C. J., Wu, C., Zhang, Y., He, N., Fu, P., Wang, Z., Shang, L., Sommar, J.,

696   Sonke, J. E., Maurice, L., Guinot, B., & Feng, X. (2016). Isotopic composition of atmospheric mercury in China: New

697   evidence for sources and transformation processes in air and in vegetation. *Environmental Science and Technology*, *50*(17),

698   9362–9369. https://doi.org/10.1021/acs.est.6b01782

699 Zhang, Y., Jacob, D. J., Dutkiewicz, S., Amos, H. M., Long, M. S., & Sunderland, E. M. (2015). Biogeochemical drivers of the

700   fate of riverine mercury discharged to the global and Arctic oceans. *Global Biogeochemical Cycles*, *29*(6), 854–864.

701   https://doi.org/10.1002/2015GB005124

702 Zheng, W., Obrist, D., Weis, D., & Bergquist, B. A. (2016). Mercury isotope compositions across North American forests.

703   *Global Biogeochemical Cycles*, *30*(10), 1475–1492. https://doi.org/10.1002/2015GB005323

704 Zhou, J., & Obrist, D. (2021). Global Mercury Assimilation by Vegetation. *Environmental Science and Technology*, *55*(20),

705   14245–14257. https://doi.org/10.1021/acs.est.1c03530

706 Zhou, J., Obrist, D., Dastoor, A., Jiskra, M., & Ryjkov, A. (2021). Vegetation uptake of mercury and impacts on global cycling.

707   *Nature Reviews Earth & Environment*, *2*(4), 269–284. https://doi.org/10.1038/s43017-021-00146-y

708

709

Figures and tables
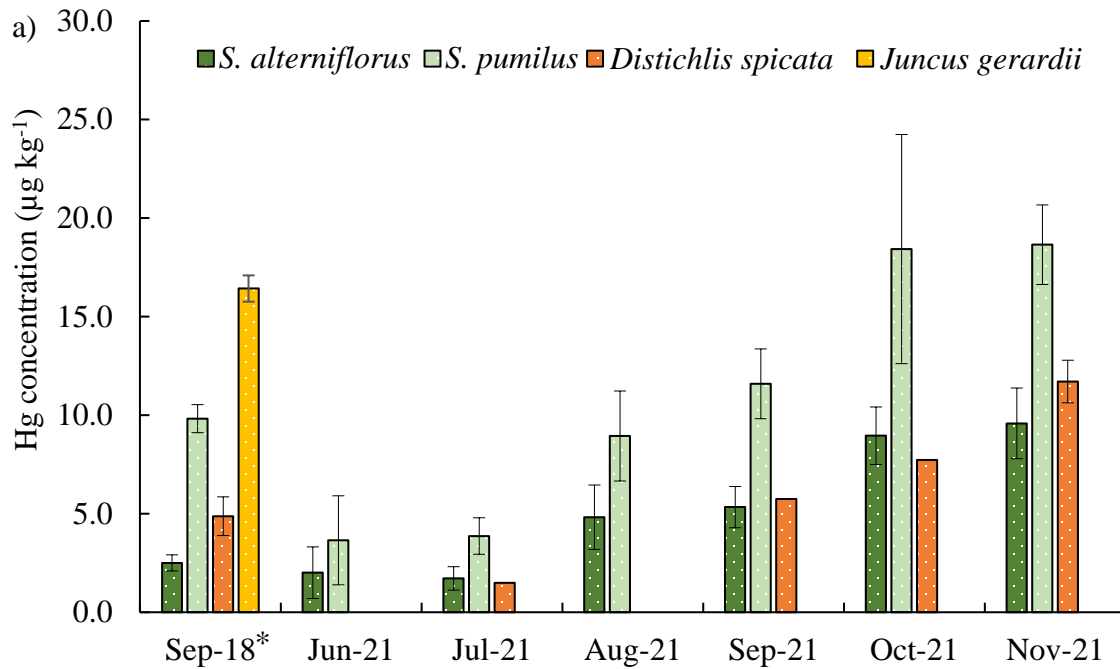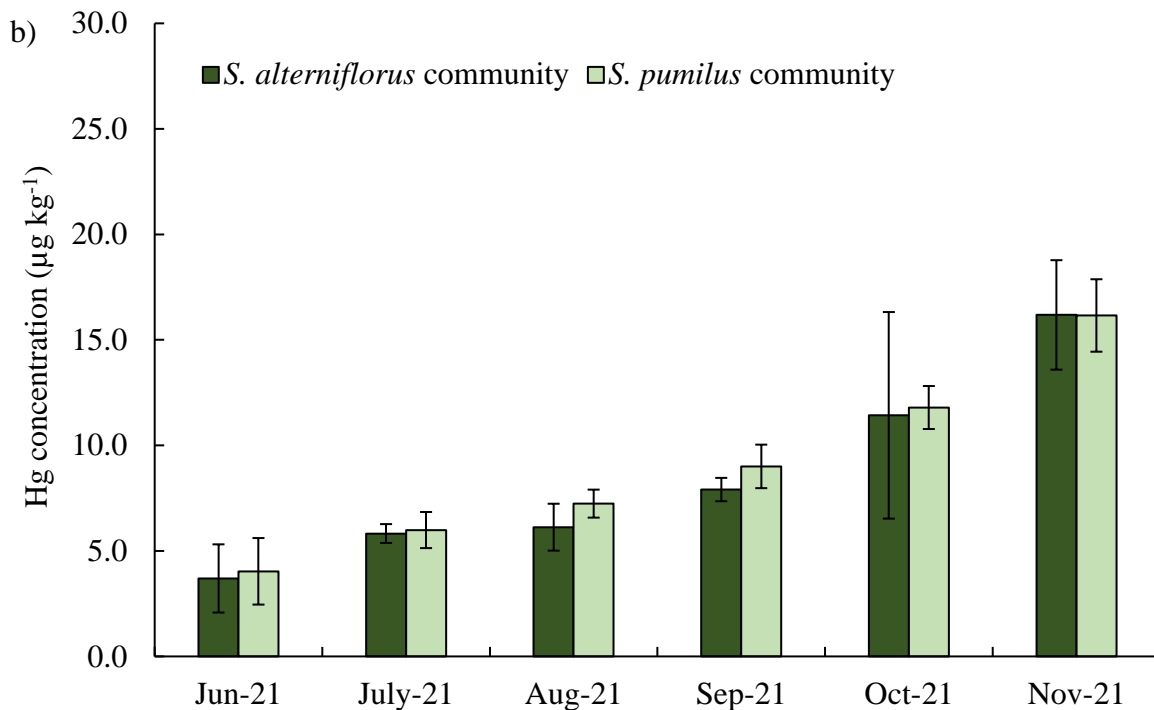
Figure 1. Seasonal Hg concentrations of the four dominated salt marsh live plant species in 2018 and 2021 a), and seasonal Hg concentrations of the *S. alterniflorus* and *S. pumilus* communities in 2021 b). Different colors indicate different plant species. Standard errors indicate four replicates. *: Standard errors indicate duplicates for a sample.

731
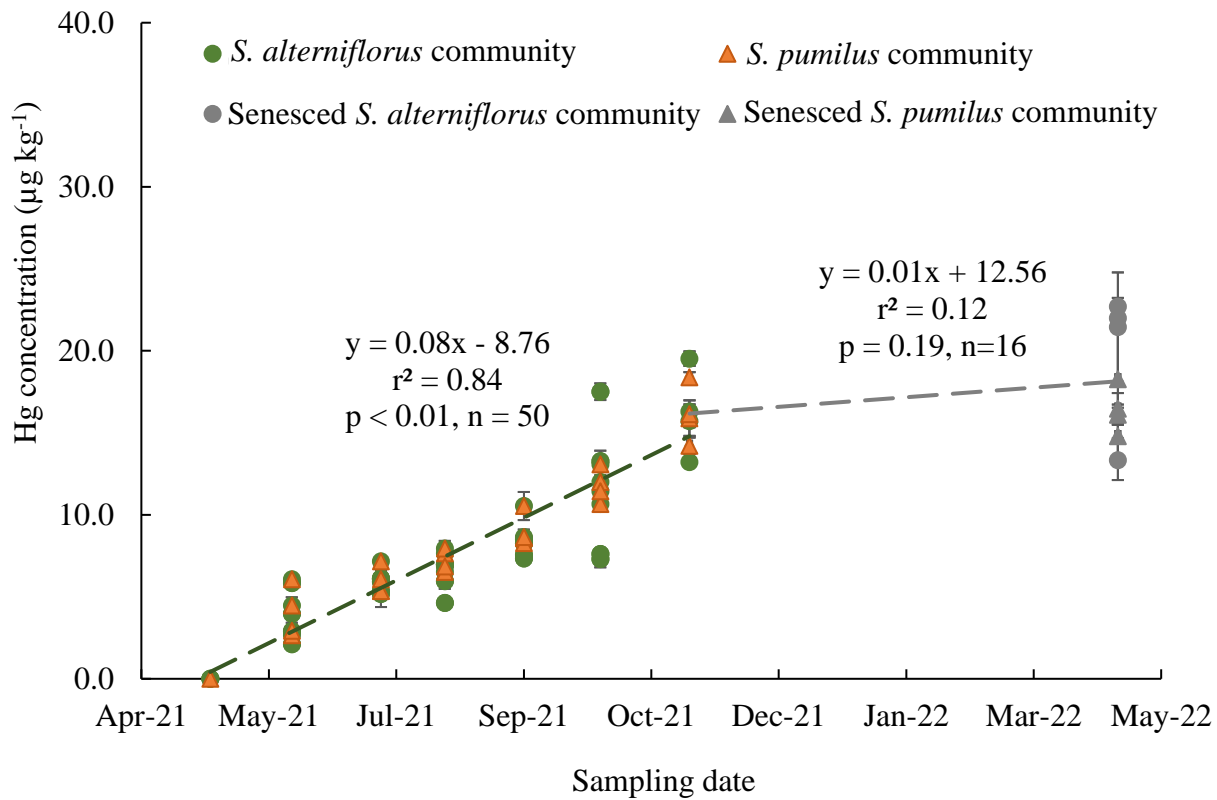
Figure 2. Hg concentrations of live and senesced aboveground biomass of *S. alterniflorus* and *S. pumilus* communities corresponds with sampling dates in 2021. Green circles indicate live *S. alterniflorus* communities, orange triangles indicate live *S. pumilus* communities, grey circles indicate senesced S. alterniflorus communities, and grey triangles indicate senesced *S. pumilus* communities. Standard errors indicate four replicates. Note that data in April 2021 was extrapolated and set to zero based on phenological observations that showed no presence of live biomass at this time.

737

738

739
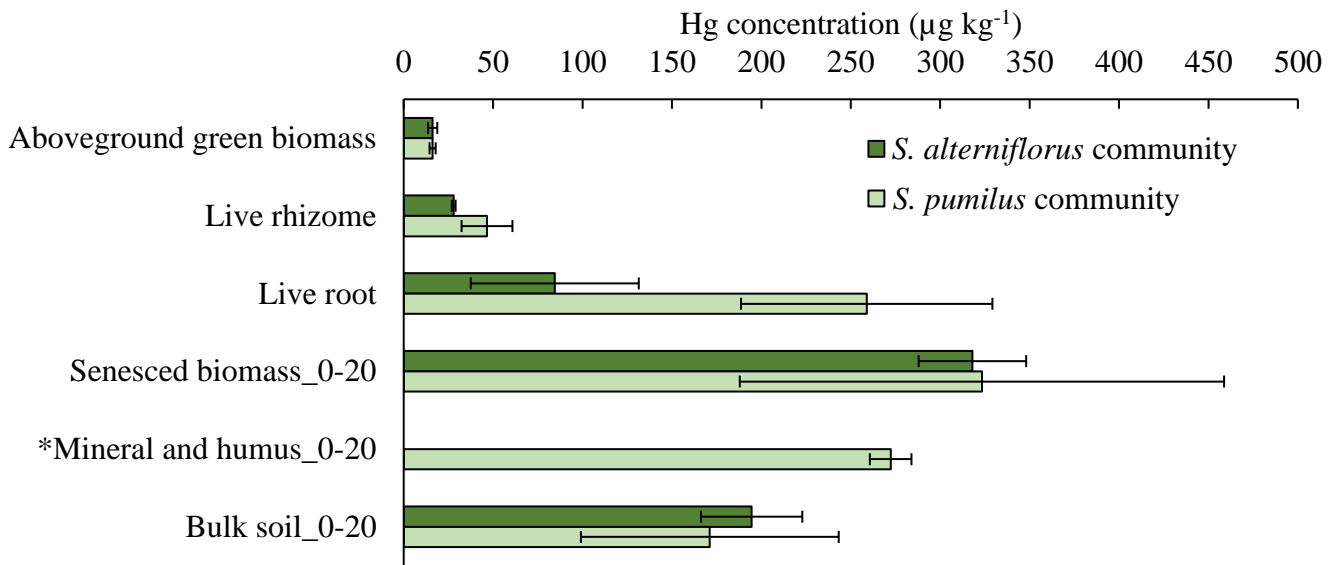
Figure 3. Hg concentrations in live above- and belowground biomass of *S. alterniflorus* and S. pumilus communities, as well as Hg concentrations of minerals and humus and bulk soils up to depth of 20cm covered by these two plant species. Dark green columns denote *S. alterniflorus* community, light green columns denote S. pumilus community. Standard errors indicate multiple sample analysis. *Hg concentration in mineral and humus only present one site covered by S. pumilus, and standard errors are duplicates.

744

745
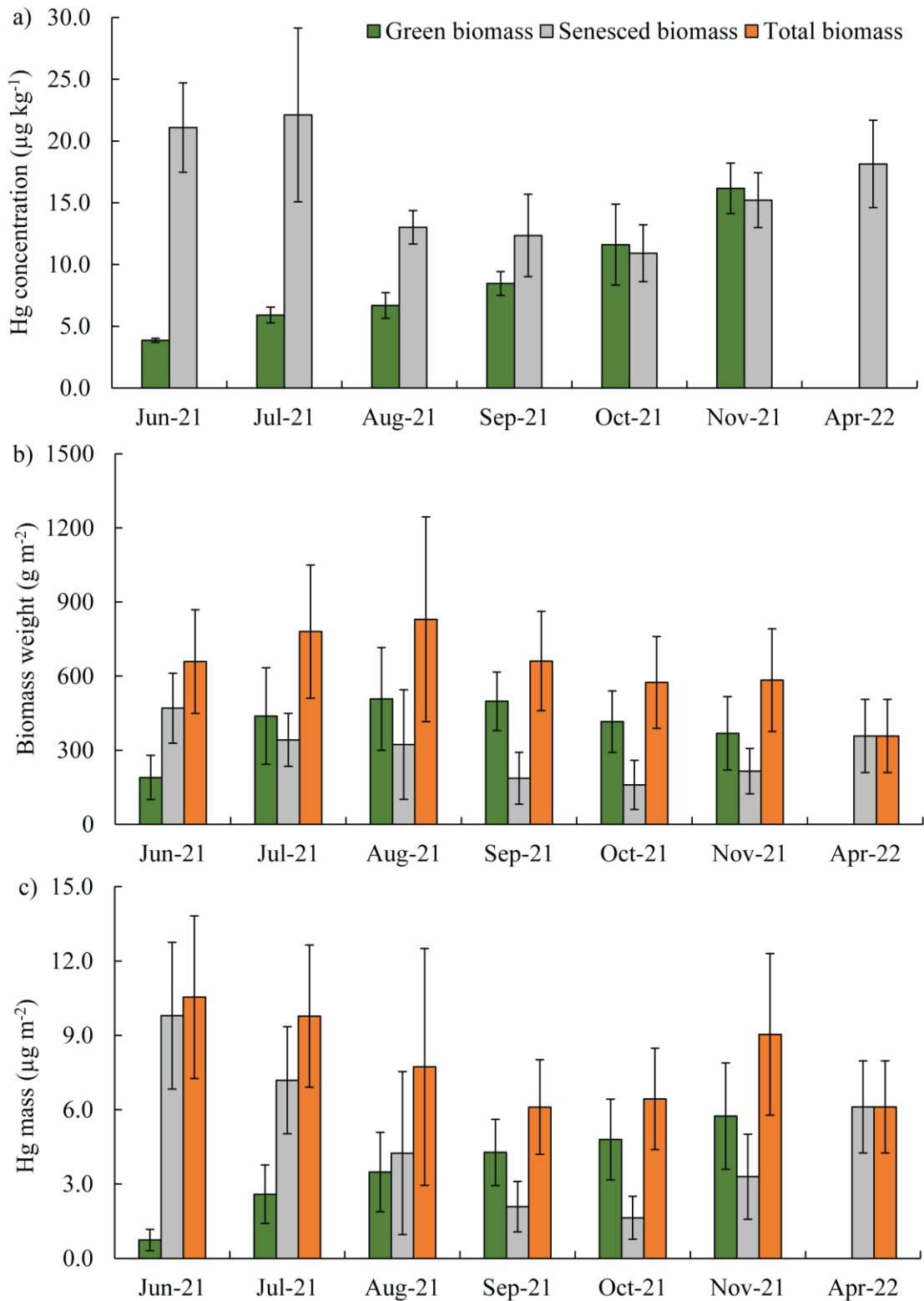
Figure 4 Seasonal patterns of Hg concentrations a), biomass dry weight b), and Hg mass c) in aboveground live and senesced biomass from June 2021 to April 2022. The green columns represent live biomass, grey columns represent senesced biomass, and orange columns represent total biomass weight and Hg mass of adding live and senesced biomass. Standard errors indicate four replicates. *: no live biomass was visible in April 2022 so that senesced biomass equals total biomass

750

751
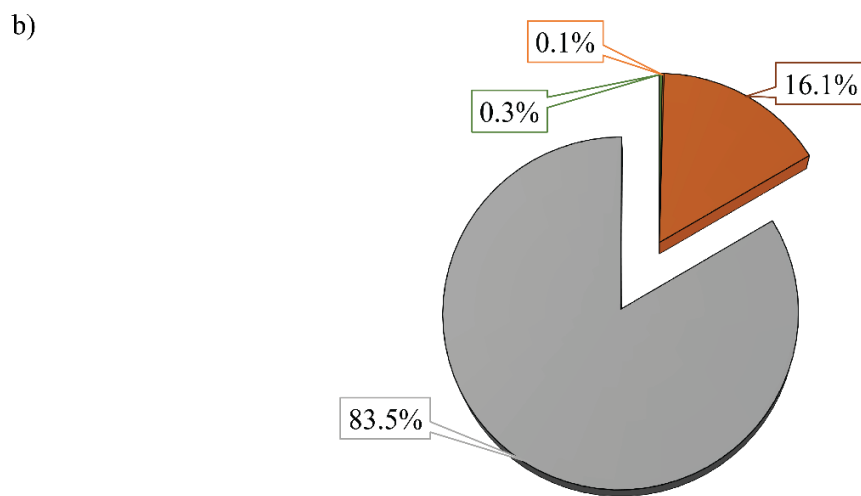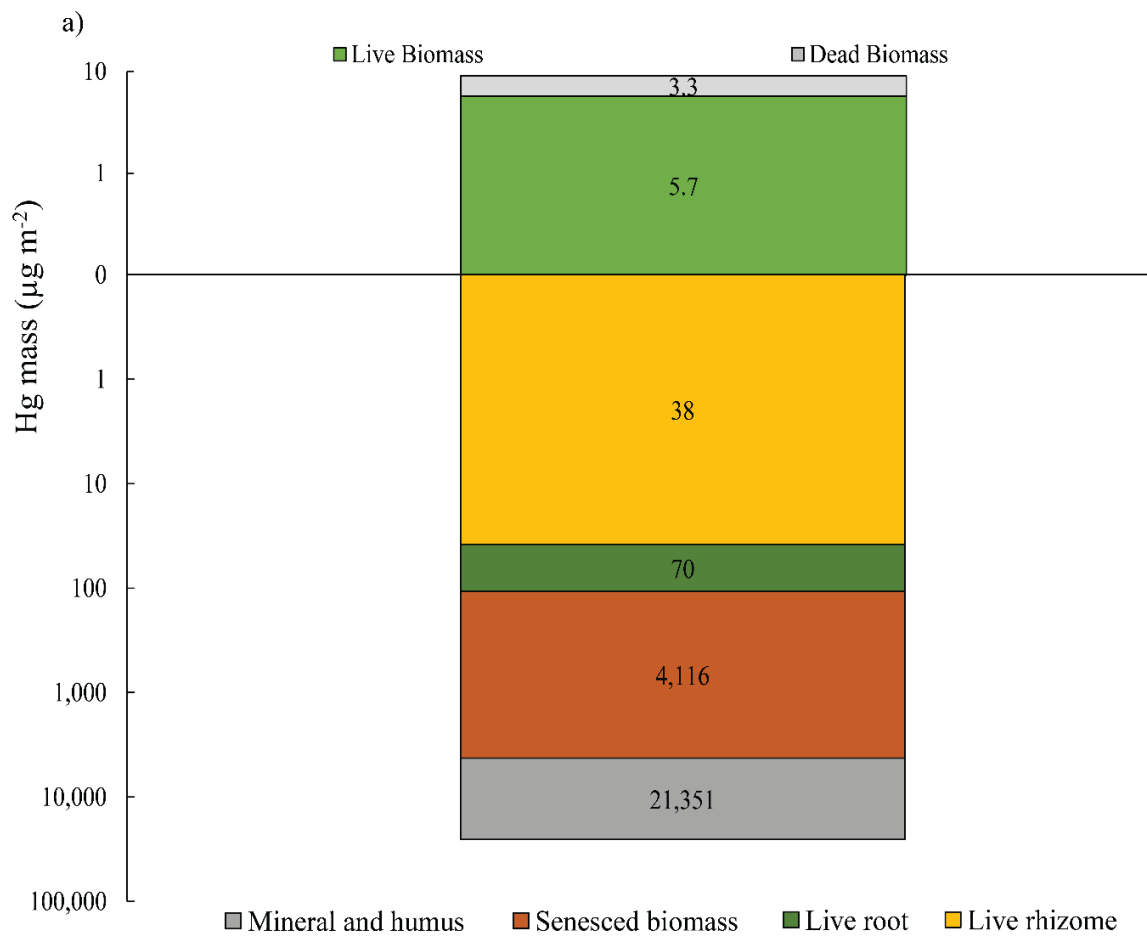
Figure 5. Hg mass of above- and belowground biomass, including live and senesced biomass, and mineral and humus fractions in a soil depth of 40cm, a), and percentages of Hg mass contribution from belowground sections to the Hg soil pool of a soil depth of 40cm, b). Different colors indicate of different sections of the marsh.

755

756
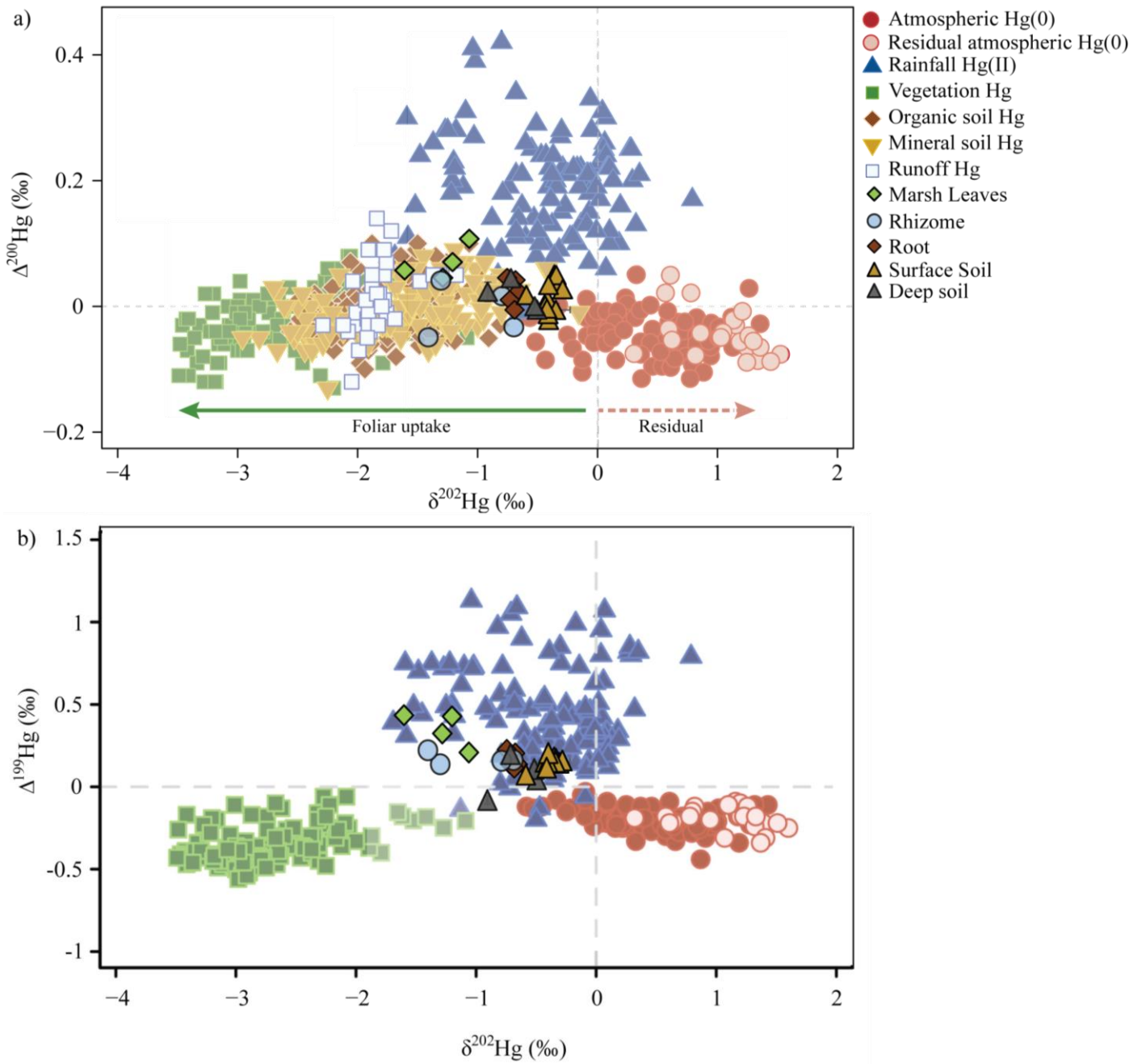
757

758 Figure 6. Hg isotopes in salt marsh plants and soils, and foliage a) of Δ^{200}Hg and δ^{202}Hg, and b) of Δ^{199}Hg and δ^{202}Hg. Composition of
759 Hg sources in marsh vegetation and soils (surface and deep soil layers), and all previously published currently available isotope data of
760 sources of Hg in vegetation and in terrestrial sinks, atmospheric Hg(0) and Hg(II) sources (Zhou et al., 2021), plotted as a) even-mass-
761 independent (Δ^{200}Hg) versus mass- dependent (δ^{202}Hg) isotopes a) and b) odd-mass-independent (Δ^{199}Hg) versus mass- dependent
762 (δ^{202}Hg) isotopes.

763

764

765
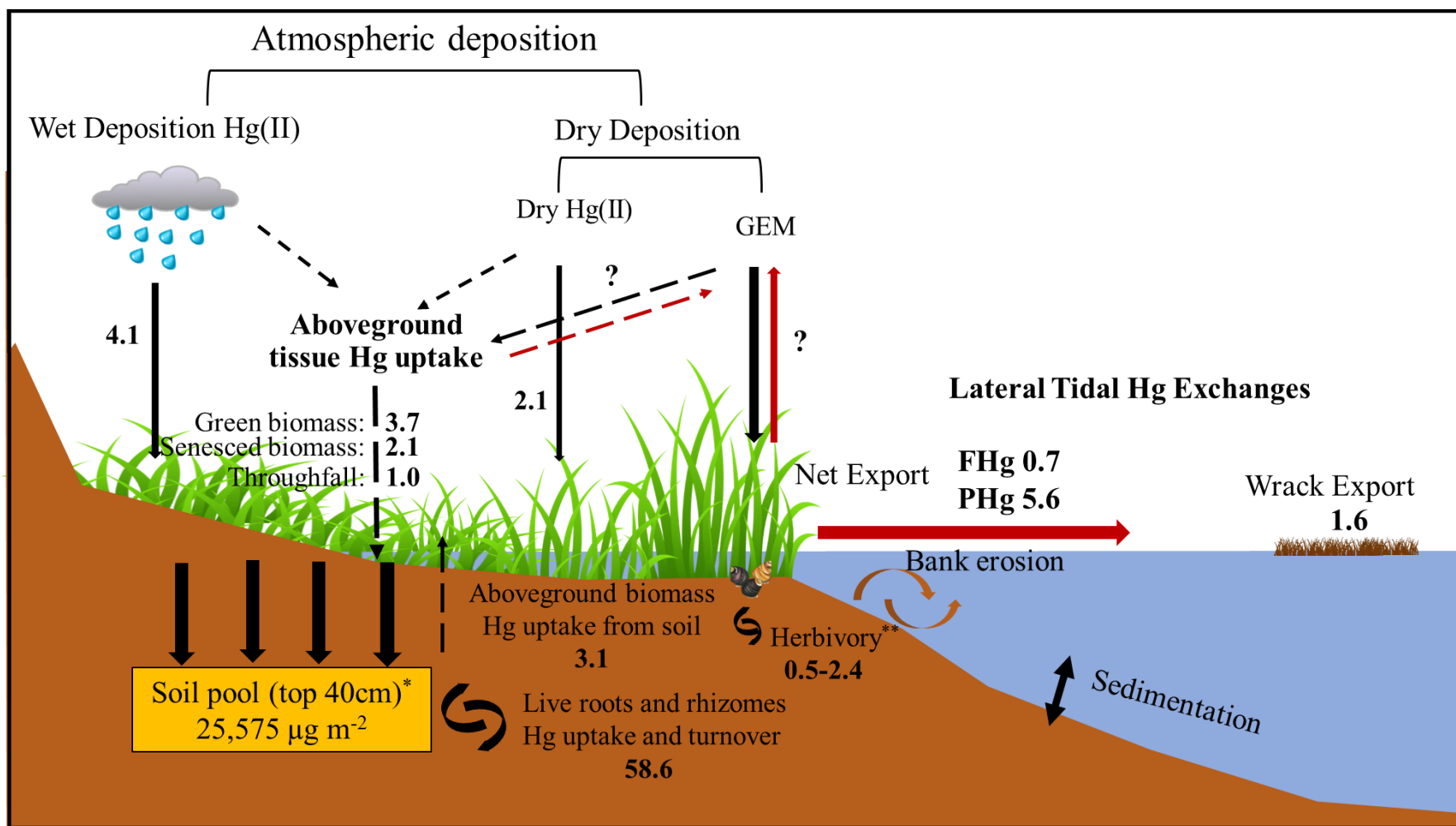
Figure 7. Hg mass balance of the study salt marsh ecosystem. The values shown mostly represent the median Hg flux values with unit of μg m^{-2} yr^{-1}, except for the soil pool*, which represents an averaged value, and herbivory**, which indicates a range. The red arrows indicate the emission of Hg back to the atmosphere and its export out of the salt marsh. The dashed arrows represent Hg fluxes related to aboveground biomass

769 **Table 1 Hg mass balance of the study salt marsh ecosystem.**

	Category	Item	Hg flux ($\mu g\ m^{-2}\ yr^{-1}$)	Percent of Hg sources	Reference	Hg fluxes scaled to the marsh ($kg\ yr^{-1}$)*
Present-day Hg Mass Balance (total inputs minus exports)	Deposition	Green aboveground biomass	3.7±1.4 (1.3-5.0)	65% atmospheric Hg	This study	0.15 (0.05-0.20)
		Senesced aboveground biomass	2.1±1.1 (1.2-4.7)	65% atmospheric Hg	This study	0.08 (0.05-0.19)
		Total aboveground biomass	5.9±2.1 (3.1-9.7)	65% atmospheric Hg	This study	0.24 (0.12-0.39)
		Throughfall	1.0±0.4 (0.5-1.6)	100% atmospheric Hg	This study	0.04 (0.02-0.06)
		Wet Hg(II)	4.1 (2.9-5.2)	100% atmospheric Hg	(Engle et al. 2010, NADP, 2017)	0.16 (0.12- 0.21)
		Dry Hg(II)	2.1 (1.2-3.0)	100% atmospheric Hg	(Engle et al., 2010, Obrist et al., 2021)	0.08 (0.05-0.12)
	Total		13.1 (7.7-19.5)		This study	0.52 (0.31-0.78)
	Export	Tidal export dissolved Hg	0.7	100% marsh soil Hg	Wang and Obrist, 2022	0.03
		Tidal export particulate Hg	5.6	100% marsh soil Hg	Wang and Obrist, 2023	0.22
		Wrack	1.6 (1.4-1.7)	100% marsh plants	This study	0.06 (0.06-0.07)
	Total		7.9 (7.7 - 8.0)		This study	0.32 (0.31-0.32)
	Net mass accumulation (estimated total deposition – total export)		**5.2 (0-11.5)**		**This study**	**0.21 (0.0-0.46)**
	Internal Cycling	Green aboveground biomass	1.9±0.7 (0.7-2.6)	35% soil Hg	This study	0.08 (0.03-0.10)
		Senesced aboveground biomass	1.1±0.6 (0.6-2.5)	35% soil Hg	This study	0.04 (0.02-0.10)
		Total aboveground biomass	3.1±1.1 (1.6-5.1)	35% soil Hg	This study	0.12 (0.06-0.20)
		Roots and rhizomes	58.6 (19.5-253.8)	90% soil Hg	This study	2.3 (0.8-10.2)
		Herbivory	0.5-2.4	100% marsh plants	This study	
		Item	Hg mass ($\mu g\ m^{-2}$)	Percent of Hg sources	Reference	Hg mass scaled to the marsh (kg)*
Total Soil Hg Mass		**Soil Hg mass top 40 cm**	25,575±14,409 (16,127-46,997)		This study	1,023±576 (645-1880)

770 * Salt marsh area (vegetated): 40 km^2